REPORT DOCUMENTATION PAGE

Form Approved
OMB No. 0704-0188

1. AGENCY USE ONLY (Leave blank)	2. REPORT DATE	3. REPORT TYPE AND DATES COVERED
	1-18-94	Annual 10/1/92 - 9/30/93

4. TITLE AND SUBTITLE
Three Dimensional Transient Analysis of Microstrip Circuits in Multilayered Anisotropic Media

5. FUNDING NUMBERS
N00014-90-J-1002
4143124-05

6. AUTHOR(S)
Prof. J.A. Kong

7. PERFORMING ORGANIZATION NAME(S) AND ADDRESS(ES)
Research Laboratory of Electronics
Massachusetts Institute of Technology
77 Massachusetts Avenue
Cambridge, MA 02139

8. PERFORMING ORGANIZATION REPORT NUMBER

9. SPONSORING/MONITORING AGENCY NAME(S) AND ADDRESS(ES)
Office of Naval Research
800 North Quincy St.
Arlington, VA 22217

10. SPONSORING/MONITORING AGENCY REPORT NUMBER

11. SUPPLEMENTARY NOTES
The view, opinions and/or findings contained in this report are those of the author(s) and should not be construed as an official Department of the Army position, policy, or decision, unless so designated by other documentation.

12a. DISTRIBUTION/AVAILABILITY STATEMENT
Approved for public release; distribution unlimited.

12b. DISTRIBUTION CODE

13. ABSTRACT *(Maximum 200 words)*

Work by Prof. Kong and his collaborators is summarized here

14. SUBJECT TERMS			15. NUMBER OF PAGES
			16. PRICE CODE
17. SECURITY CLASSIFICATION OF REPORT	18. SECURITY CLASSIFICATION OF THIS PAGE	19. SECURITY CLASSIFICATION OF ABSTRACT	20. LIMITATION OF ABSTRACT
UNCLASSIFIED	UNCLASSIFIED	UNCLASSIFIED	UL

NSN 7540-01-280-5500

Standard Form 298 (Rev. 2-89)
Prescribed by ANSI Std 239-18
298-102

GENERAL INSTRUCTIONS FOR COMPLETING SF 298

The Report Documentation Page (RDP) is used in announcing and cataloging reports. It is important that this information be consistent with the rest of the report, particularly the cover and title page. Instructions for filling in each block of the form follow. It is important to ***stay within the lines*** to meet ***optical scanning requirements***.

Block 1. Agency Use Only *(Leave blank)*.

Block 2. Report Date. Full publication date including day, month, and year, if available (e.g. 1 Jan 88). Must cite at least the year.

Block 3. Type of Report and Dates Covered. State whether report is interim, final, etc. If applicable, enter inclusive report dates (e.g. 10 Jun 87 - 30 Jun 88).

Block 4. Title and Subtitle. A title is taken from the part of the report that provides the most meaningful and complete information. When a report is prepared in more than one volume, repeat the primary title, add volume number, and include subtitle for the specific volume. On classified documents enter the title classification in parentheses.

Block 5. Funding Numbers. To include contract and grant numbers; may include program element number(s), project number(s), task number(s), and work unit number(s). Use the following labels:

C	- Contract	**PR**	- Project
G	- Grant	**TA**	- Task
PE	- Program Element	**WU**	- Work Unit Accession No.

Block 6. Author(s). Name(s) of person(s) responsible for writing the report, performing the research, or credited with the content of the report. If editor or compiler, this should follow the name(s).

Block 7. Performing Organization Name(s) and Address(es). Self-explanatory.

Block 8. Performing Organization Report Number. Enter the unique alphanumeric report number(s) assigned by the organization performing the report.

Block 9. Sponsoring/Monitoring Agency Name(s) and Address(es). Self-explanatory.

Block 10. Sponsoring/Monitoring Agency Report Number. *(If known)*

Block 11. Supplementary Notes. Enter information not included elsewhere such as: Prepared in cooperation with...; Trans. of...; To be published in.... When a report is revised, include a statement whether the new report supersedes or supplements the older report.

Block 12a. Distribution/Availability Statement. Denotes public availability or limitations. Cite any availability to the public. Enter additional limitations or special markings in all capitals (e.g. NOFORN, REL, ITAR).

DOD - See DoDD 5230.24, "Distribution Statements on Technical Documents."
DOE - See authorities.
NASA - See Handbook NHB 2200.2.
NTIS - Leave blank.

Block 12b. Distribution Code.

DOD - Leave blank.
DOE - Enter DOE distribution categories from the Standard Distribution for Unclassified Scientific and Technical Reports.
NASA - Leave blank.
NTIS - Leave blank.

Block 13. Abstract. Include a brief *(Maximum 200 words)* factual summary of the most significant information contained in the report.

Block 14. Subject Terms. Keywords or phrases identifying major subjects in the report.

Block 15. Number of Pages. Enter the total number of pages.

Block 16. Price Code. Enter appropriate price code *(NTIS only)*.

Blocks 17. - 19. Security Classifications. Self-explanatory. Enter U.S. Security Classification in accordance with U.S. Security Regulations (i.e., UNCLASSIFIED). If form contains classified information, stamp classification on the top and bottom of the page.

Block 20. Limitation of Abstract. This block must be completed to assign a limitation to the abstract. Enter either UL (unlimited) or SAR (same as report). An entry in this block is necessary if the abstract is to be limited. If blank, the abstract is assumed to be unlimited.

ANNUAL REPORT

Title: THREE DIMENSIONAL TRANSIENT ANALYSIS OF MICROSTRIP CIRCUITS IN MULTILAYERED ANISOTROPIC MEDIA

Sponsor by: Department of the Navy/Office of Naval Research

Contract number: N00014-90-J-1002

Research Organization: Center for Electromagnetic Theory and Applications
Research Laboratory of Electronics
Massachusetts Institute of Technology

OSP number: 72943

Principal Investigator: J. A. Kong

Period covered: October 1, 1992 — September 30, 1993

Three Dimensional Transient Analysis of Microstrip Circuits in Multilayered Anisotropic Media

Under the sponsorship of the ONR contract N00014-90-J-1002 we have published (18) refereed journal and conference papers.

In high-speed digital circuits, high frequency phenomena affects the characteristics of the interconnections. Physical discontinuities or nonuniformities in the connections may cause severe reflections when they can no longer be considered as conducting wires, but behave as transmission lines and/or waveguides. In multilayered digital circuits, vias constitute one of the most commonly-used class of interconnects. Vias are not good carriers of high-speed signals. They cause signal distortion and reflections as well as severe degradation in the high frequency components. The analysis and modeling of a single via and some quasi-static or quasi-TEM analyses of single via configurations have been carried out previously. To date, the analysis of coupled noise between adjacent vias has received very little attention. The major reasons include the complexity of multi-via structures and the difficulty of modeling and analyzing them accurately over a broad frequency range. The electromagnetic coupling between two adjacent vias in a multilayered integrated circuit is analyzed by means of equivalent magnetic frill array models incorporated with the even- and odd-mode approach. Closed-form expressions for the coupled noise on the passive via are derived. The coupling responses in the frequency domain and crosstalk waveforms in the time domain for some multilayered via structures are calculated based on these formulas. A 4-layer experimental model is constructed and measurements are taken for the transmission, reflection, and coupling responses. The measurements show good agreement with the calculated results over a frequency range of up to 18 GHz.

High frequency digital signals associated with computers and communications equip-

ment have the potential for electromagnetic interference (EMI). The need for compliance with the radiated emissions limits established by FCC and other regulatory agencies for such equipment have led to increased interest in understanding and minimizing EM radiation. As clock speeds increase beyond 100 MHz and edge-rates fall into the sub-nanosecond range, the EMC engineer is faced with FCC tests for frequencies beyond 1 GHz and the prospect of increased energy for frequencies in the hundreds of megahertz range. The modules-on-backplane configuration is a common assembly scheme for computers. Embedded in these modules and backplane are reference planes which could be as large as tens of centimeters. The reference planes configuration is of interest because the resonant frequencies begin in the low hundreds of megahertz, given typical dimensions. The voltage levels on such reference planes are subject to noise fluctuations (reference noise) originating from disturbances such as inductive discontinuities at connector pins. The increase in power requirements and in the number of simultaneous switching circuits is likely to result in stronger noise sources. A simplified model is used to analyze the modules-on-backplane configuration. Conducting planes model the modules and the backplane. A generator, which is positioned at the module and backplane interface, models the inductive voltage, as a noise source, developed across the module-backplane connector. The *finite-difference time-domain* (FD-TD) technique, which is based on the discretization of the Maxwell's equations, is employed in this analysis. Nodal electric and magnetic fields are computed on a rectangular grid within a computational domain subject to appropriate boundary and initial conditions. An absorbing boundary condition is enforced on the outer boundary of the computational domain and approximately simulates unbounded space. In the implementation of the FD-TD technique, the areas of concern addressed include the modeling of the excitation as a coaxial line probe and the use of Prony's method to obtain late time responses of the fields for highly resonant configurations. Radiation impedances are obtained from the voltages and currents on the probe and radiation patterns are calculated using Huygens' principle. Experimental verification is made on physical structures com-

patible with simulation models. The focus is on correlating computed resonant frequencies and radiation impedances with those deduced from S-parameter measurements taken on a network analyzer. Radiation impedances as functions of frequency are presented for various configurations. Such variations include changing the number of modules and the dimensions and spacings of modules and backplane and the addition of conducting panels to model the shielding or enclosure environment. This study provides basic information pertaining to the acceptability of noise levels in the interconnect environment for EMI-related considerations. Through the examination of a variety of configurations it will also affect system-level packaging and assembly decisions.

Millimeter and submillimeter transmission structures are dominated by dielectric waveguides. At these frequency bands, conventional microstrip transmission structures such as microstrip line, coplanar line, slot line and finline all suffer from severe ohmic and radiation losses. Analytical techniques for studying dielectric waveguide structures include the full-wave integral equation formulations (both spectral and spatial domain) and the finite difference time-domain (FDTD) method. Compared to the integral equation methods, the FDTD method is more straightforward to formulate and provides an alternative path to analyze both time and frequency domain response in the presence of complex structures such as discontinuities. In this study, electromagnetic pulse propagation in single and coupled dielectric rib waveguide embedded in a three-layer stratified dielectric medium is simulated and analyzed using the FDTD technique. Time domain transient response of a modulated gaussian pulse is observed in the simulation. We first examine pulse dispersion, attenuation and coupling characteristics for the transmission line structure. Results are found to be in good agreement with those obtained from integral equation methods. We also extend the study to an optical rib waveguide with a bend discontinuity. The FDTD simulation is used to predict the electromagnetic leakage attributed to the discontinuity. One of the problems facing the FDTD technique for the dielectric waveguide problem is the proper absorbing boundary condition. Existing boundary conditions such as the Mur,

Enquist-Majda condition work best when wave incident angle is normal to the boundary; which is generally not the case for dielectric waveguides. A comparison between different conditions will also be presented.

The use of equipment enclosures to shield against emissions and external energy is a common practice. Efforts range from metal impregnated plastics to thick steel panels incorporating waveguide design in air vents. The choice of complexity depends on system performance and application. The question has often been raised as to whether high field intensities within such enclosures will affect equipment performance. Clearly this is increasingly pertinent in cases of heavy shielding where resonator-like structures with high quality factors (Q) result. Moreover, in these cases, any energy leakage may be highly frequency selective with substantial associated field strength. The primary motivation for studying such structures is that computers are now operating at faster speeds and consuming more power resulting in significantly increased levels of power at higher frequencies. Also typical metallic enclosure configurations have dimensions which are electrically resonant at frequencies in the hundreds of megahertz range. We focus on the use of resistive material within the enclosure walls for absorbing some of the contained RF energy, thereby avoiding high Q enclosures and reducing the likelihood of significant field buildup within the enclosure. The energy leakage from perforations on the walls is also being considered. The radiation properties of these structures are observed by varying the number, size and position of the holes in the enclosure. The finite-difference time-domain (FD-TD) technique is used in analyzing this problem and the metrics are total radiated power and field patterns within the enclosure. The excitation sources are line current source for the two-dimensional models and dipoles for the three-dimensional cases. A Gaussian amplitude is assumed in order to obtain multifrequency characteristics and to exhibit the resonance properties of the model. In addition to the radiated power through the apertures, the power absorbed in the resistive material is also calculated.

A new method based on the wave transmission matrix is presented to deal with nonuniform multiconductor line system. This method has not only the ability of handling nonuniformity, but also the advantage of handling nonlinearity efficiently. The wave transmission matrix is employed to characterize the multiconductor transmission lines and the telegrapher equations, therefore, can easily be turned into algebraic equations. The nonuniform transmission line is treated as many small segments of uniform transmission lines connected in cascade. The formulation for this method is described in detail. Calculation approaches are discussed. Numerical results are presented and comparison of them with previous work confirms the validity of the method.

A macroscopic model is proposed for nonlinear electromagnetic phenomena in superconductors. Nonlinear constitutive relations are derived by modifying the linear London's equations. The superelectron number density as a function of applied macroscopic current density, $n_s(J)$, is derived from a distribution of electron velocities at a certain temperature T. At temperature $T \neq 0$K, the function $n_s(J)$ has a smooth variation near the macroscopic critical current density J_C. Agreement has been found between this $n_s(J,T)$ model and the temperature dependence of n_s in the two-fluid model. The nonlinear conductivities $\sigma_s(J)$ and $\sigma_n(J)$ are obtained from the London's equation with the modified $n_s(J)$ function. Nonlinear resistance $R(I)$, kinetic inductance $L_k(I)$ and surface impedance $Z_s(I)$ in thin wire, slab, and strip geometries are calculated.

The finite difference-time domain (FD-TD) technique is applied to the solution of Maxwell's equations. A computer program, which can be used to simulate and study numerous electromagnetic phenomena, is developed and implemented on a 386-class personal computer. The FD-TD technique is a useful tool for students in electromagnetics. The technique is flexible and can be applied to many basic EM scattering and radiation problems. Because field solutions are found as a function of time, visualization of the propagation of the EM fields is possible. The FD-TD technique is implemented for a

two-dimensional rectangular grid in conjunction with a second-order absorbing boundary condition. Both E- and H-field polarizations are analyzed. Finite objects consisting of dielectric, magnetic and conducting materials, and perfectly conducting infinite ground planes are modeled. Plane wave and line current sources are implemented. In addition to the capability of animating the propagation of the EM fields, radiation and scattering patterns can be generated.

A methodology developed to handle dispersive materials in the time domain is extended to model the dispersive characteristics of the impedance boundary condition used for a thin layer coating over perfect conductors. The impedance boundary condition is first approximated as a rational function of frequency. This rational function is then transformed to a time domain equation, resulting in a partial differential equation in space and time. Discretization of the time domain model to efficiently handle the thin layer coating is presented in the context of the finite-difference time-domain (FD-TD) technique. The methodology is verified by solving a one-dimensional problem using the FD-TD technique and comparing with the analytical results.

To understand the physical meaning of rational reflection coefficients in inverse-scattering theory for optical waveguide design, we studied the relationship between the poles of the transverse reflection coefficient and the modes in inhomogeneous dielectrics. By using a stratified-medium formulation we showed that these poles of the spectral reflection coefficient satisfy the same equation as the guidance condition in inhomogeneous waveguides. Therefore, in terms of wave numbers, the poles are the same as the discrete modes in the waveguide. The radiation modes have continuous real values of transverse wave numbers and are represented by the branch cut on the complex plane. Based on these results, applications of the Gel'fand-Levitan-Marchenko theory to optical waveguide synthesis with the rational function representation of the transverse reflection coefficient are discussed.

The coupled-wave theory is generalized to analyze the diffraction of waves by chiral gratings for arbitrary angles of incidence and polarizations. Numerical results for the Stokes parameters of diffracted Floquet modes versus the thickness of chiral gratings with various chiralities are calculated. Both horizontal and vertical incidences are considered for illustration. The diffracted waves from chiral gratings are in general elliptically polarized; and in some particular instances, it is possible for chiral gratings to convert a linearly polarized incident field into two nearly circularly polarized Floquet modes propagating in different directions.

A general spectral domain formulation to the problem of radiation of arbitrary distribution of sources embedded in a horizontally stratified arbitrary magnetized linear plasma is developed. The fields are obtained in terms of electric and magnetic type dyadic Green's functions. The formulation is considerably simplified by using the kDB system of coordinates in conjunction with the Fourier transform. The distributional singular behavior of the various dyadic Green's functions in the source region is investigated and taken into account by extracting the delta function singularities. Finally, the fields in any arbitrary layer are obtained in terms of appropriately defined global upward and downward reflection and transmission matrices.

We investigated a method for the calculation of the current distribution, resistance, and inductance matrices for a system of coupled superconducting transmission lines having finite rectangular cross section. These calculations allow accurate characterization of both high-T_c and low-T_c superconducting strip transmission lines. For a single stripline geometry with finite ground planes, the current distribution, resistance, inductance, and kinetic inductance are calculated as a function of the penetration depth for various film thickness. These calculations are then used to determine the penetration depth for Nb, NbN, and $YBa_2Cu_3O_{7-x}$ superconducting thin films from the measured temperature dependence of the resonant frequency of a stripline resonator. The calculations are also used to convert

measured temperature dependence of the quality factor to the intrinsic surface resistance as a function of temperature for a Nb stripline resonator.

The electromagnetic radiation from a VLSI chip package and heatsink structure is analysed by means of the finite-difference time-domain (FD-TD) method. The FD-TD algorithm implemented incorporates a multi-zone gridding scheme to accommodate fine grid cells in the vicinity of the heatsink and package cavity and sparse gridding in the remainder of the computational domain. The issues pertaining to the effects of the heatsink in influencing the overall radiating capacity of the configuration are addressed. Analyses are facilitated by using simplified heatsink models and by using dipole elements as sources of electromagnetic energy to model the VLSI chip. The potential for enhancement of spurious emissions by the heatsink structure is examined. For heatsinks of typical dimensions, resonance is possible within the low gigahertz frequency range.

Because the effects of diffraction during proximity-print x-ray lithography are of critical importance, a number of previous researchers have attempted to calculate the diffraction patterns and minimum achievable feature sizes as a function of wavelength and gap. Work to date has assumed that scalar diffraction theory is applicable–as calculated, for example, by the Rayleigh-Sommerfeld formulation–and that Kirchhoff boundary conditions can be applied. Kirchhoff boundary conditions assume that the fields (amplitude and phase) are constant in the open regions between absorbers, and a different constant in regions just under the absorbers (i.e., that there are no fringing fields). An x-ray absorber is, however, best described as a lossy dielectric that is tens or hundreds of wavelengths tall, and hence Kirchhoff boundary conditions are unsuitable. We have instead used two numerical techniques to calculate accurate diffracted fields from gold absorbers for two cases: a 30 nm-wide line at $\lambda = 4.5$ nm, and a 100 nm-wide line at $\lambda = 1.3$ nm. We show that the use of Kirchhoff boundary conditions introduces unphysically high spatial frequencies into the diffracted fields. The suppression of these frequencies–which occurs

naturally without the need to introduce an extended source or broad spectrum–improves exposure latitude for mask features near 0.1 μm and below.

In order to understand the physical meaning of rational reflection coefficients in one-dimensional inverse scattering theory for optical waveguide design, we have studied the relation between the poles of the transverse reflection coefficient and the modes in inhomogeneous dielectrics. By using a stratified medium model it is shown that these poles of the reflection coefficient have a one-to-one correspondence to the discrete modes, which are the guided and leaky modes. The radiation modes have continuous real values of transverse wave numbers and are not represented by the poles of the reflection coefficient. Based on these results, applications of the Gel'fand-Levitan-Marchenko theory to optical waveguide synthesis with the rational function representation of the transverse reflection coefficient are investigated.

In compact modules of high performance computers, signal transmission lines between integrated circuit chips are embedded in multilayered dielectric medium. These signal lines are usually placed in different layers and run perpendicular to each other. The interaction between the orthogonal crossing lines and the signal line affects its propagation characteristics and may cause considerable signal distortion.

The interaction of a pair of crossing lines in isotropic medium has been studied using a time-domain approach, where coupling is described qualitatively. This method becomes computationally expensive when the number of crossing lines increases. With many identical crossing strips uniformly distributed above the signal line, the transmission properties are characterized by stopbands due to the periodicity of the structure. Periodic structure have been investigated using frequency-domain methods. Periodically nonuniform microstrip lines in an enclosure are analyzed on the basis of a numerical field calculation. A technique based on the network-analytical formulism of electromagnetic fields has been used to analyze striplines and finlines with periodic stubs. The propagation characteristics

of waves along a periodic array of parallel signal lines in a multilayered isotropic structure in the presence of a periodically perforated ground plane and that in a mesh-plane environment have been studied. More recently, the effect of the geometrical properties on the propagation characteristics of strip lines with periodic crossing strips embedded in a shielded one-layer isotropic medium have been investigated. Both open and closed multilayered uniaxially anisotropic structures are considered. A full-wave analysis is used to study the propagation characteristics of a microstrip line in the presence of crossing strips. The signal line and the crossing strips are assumed to be located in two arbitrary layers of a stratified uniaxially anisotropic medium. An integral equation formulation using dyadic Green's functions in the periodically loaded structure is derived. Galerkin's method is then used to obtain the eigenvalue equation for the propagation constant. The effects of anisotropy on the stopband properties are investigated. Numerical results for open and shielded three-layer uniaxially anisotropic media are presented.

For microwave integrated circuit applications, the characteristics of interconnects have been investigated for the propagation modes, time response, crosstalk, coupling, delay, etc. In these analyses, it is assumed that quasi-TEM modes are guided along the multiconductor transmission lines. The analysis were performed for arbitrary number of transmission lines where the load and the source conditions were presented in terms of the modal reflection and transmission coefficient matrices.

To perform the quasi-TEM analysis, the capacitance matrix for the multiconductor transmission line has to be obtained first. Both the spectral and the spatial domain methods have been proposed to calculate the capacitance matrix. In the spectral domain methods, two side walls are used to enclose the whole transmission line structure, and the thickness of the strip lines has not been considered. In using the spatial domain method, the structure has to be truncated to a finite extent to make the numerical implementation feasible. The infinite extent of the structure was also incorporated, but only a two-layer

medium was considered.

In practical microwave integrated circuits, the dielectric loss due to the substrate and the conductor loss due to the metallic strips are also studied in the analysis of circuit performances.

Based on the scalar Green's function, a set of coupled integral equations is obtained for the charge distribution on the strip surfaces. Pulse basis functions and a point-matching scheme is used to solve numerically the set of integral equations for the charge distribution, and hence the capacitance matrix. The duality between the electrostatic formulation and the magnetostatic one is applied to calculate the inductance matrix. The conductance matrix is obtained by using the duality between the electrostatic problem and the current field problem. A perturbation method is used to calculate the resistance matrix.

Finally, a transmission line analysis is derived to obtain the transfer matrix for multiconductor uniform lines, which significantly reduces the effort in treating the load and the source conditions. Transient responses are obtained by using the Fourier transform. The results for two coupled lines are obtained.

With the ever increasing speed and density of modern integrated circuits, the need for electromagnetic wave analysis of phenomena such as the propagation of transient signals, especially the distortion of signal pulses, becomes crucial. One of the most important causes of pulse distortion is the frequency dependence of conductor loss, which is caused by the "skin effect", and which can be incorporated into the circuit models for transmission lines as frequency-dependent resistance and inductance per unit length. Efficient and accurate algorithms for calculating these parameters are increasingly important.

We have developed a hybrid cross-section finite element/coupled integral equation method. The technique is a combination of a cross-section finite element method, which is best for high frequencies. An interpolation between the results of these two methods gives

very good results over the entire frequency range, even when few basis functions are used.

In the cross-section method, we divide each conductor into triangular patches and choose one of the patches from the return conductor to be our reference. We then calculate the resistance and inductance matrices for the patches. Using two conditions on the system, that the total current in each wire is the sum of the currents in the patches, and that the voltage on each patch in a wire must be the same (no transverse currents), we can reduce the matrices for the patches to the matrices for the wires. In the Weeks method, the patches are rectangles, and the quadruple integral is done quite easily in closed form. However, it is also possible to evaluate the quadruple integral in closed form for triangular patches, although the mathematics leading to this result is quite involved, and the final form of the answer is complicated. We therefore use triangular patches as the most flexible means of modelling conductors with arbitrary cross-sections; polygons are covered exactly, and we are able to model quite closely other shapes, such as circles.

As frequency increases, the need to keep the uniform current approximation valid in the patches requires either the addition of many more patches as the skin depth decreases, or a redistribution of the existing patches to the surface, where the current is. However, changing the distribution of patches makes it necessary to recalculate the resistance and inductance matrices of the patches, thus increasing the computation time. Since we use a surface integral equation method for high frequencies, we do not change the distribution of the triangular patches for the cross-section method as we increase the frequency.

For high frequencies, we use a coupled surface integral equation technique. Under the quasi-TEM assumption, the frequency-dependent resistance and inductance result from the power dissipation and magnetic stored energy, which can be calculated by solving a magnetoquasistatic problem, with the vector potential satisfying Laplace's equation in the region outside all the conductors. The resistance and inductance are usually given by integrals of these field quantities over the cross-sections of the wires, but by using some

vector identities it is possible to convert these expressions to integrals only over the surfaces of the wires. These expressions contain only the current at the surface of each conductor, the derivative of that current normal to the surface, and constants of the vector potential. A coupled integral equation is then derived to relate these quantities through Laplace's equation and its Green's function outside the conductors and the diffusion equation and its Green's function inside the conductors. The method of moments with pulse basis functions is used to solve the integral equations. This method differs from previous work in that the calculation of resistance and inductance is based on power dissipation and stored magnetic energy, rather than on impedance ratios. It will therefore be more easily extended to structures where non-TEM propagation can occur.

For the intermediate frequency range, where the conductors are on the order of the skin depth, were found it very efficient to interpolate between the results of the cross-section and surface methods. The interpolation function was based on the average size of the conductors, measured in skin depths, and was of the form $1/(1+0.16a^2/\delta^4)$, where it a is the average cross-section of the conductors, and δ is the skin depth.

Coupled noise analysis for adjacent vias in multilayered digital circuits (Q. Gu, M. A. Tassoudji, S. Y. Poh, R. T. Shin, and J. A. Kong), Progress in Electromagnetics Research Symposium at the Jet Propulsion Laboratory, California Institute of Technology, Pasadena, California, July 12-15, 1993.

Electromagnetic radiation from modules-on-backplane configurations in computer systems (K. Li, M. A. Tassouodji, S. Y. Poh, R. T. Shin, and J. A. Kong), Progress in Electromagnetics Research Symposium at the Jet Propulsion Laboratory, California Institute of Technology, Pasadena, California, July 12-15, 1993.

Analyses of single and coupled dielectric rib waveguides and discontinuities using the finite-difference time-domain method (A. Mou, Y. E. Yang, and J. A. Kong), Progress in Electromagnetics Research Symosium at the Jet Propulsion Laboratory, California Institute of Technology, Pasadena, California, July 12-15, 1993.

Electromagnetic Fields in Metallic Enclosures Lined with Resistive Material (M. A. Tassoudji, K. Li, R. T. Shin, J. A. Kong, M. J. Tsuk), Progress in Electromagnetics Research Symposium at the Jet Propulsion Laboratory, California Institute of Technology, Pasadena, California, July 12-15, 1993.

Analysis of Nonuniform Multiconductor Transmission Line Systems - Wave Transmission Matrix Method (Q. Gu, M. A. Tassoudji, and Y. Yuan), submitted for publication in *IEEE Transactions on Circuits and Systems*, 1993.

A macroscopic model of nonlinear constitutive relations in superconductors (J. J. Xia, J. A. Kong, and R. T. Shin), accepted for publication in *IEEE Transactions on Microwave Theory and Techniques*, 1993.

Simulation of electromagnetic radiation and scattering using a finite difference-time doma·. technique (K. Li, M. A. Tassoudji, R. T. Shin, and J. A. Kong), *Computer Applications in Engineering Education*, Vol. 1, No. 1, 45–63, September/October 1992.

Time domain modeling of impedance boundary condition (C. F. Lee, R. T. Shin, and J. A. Kong), *IEEE Transactions on Microwave Theory and Techniques*, Vol. 40, No. 9, September 1992.

Inverse scattering view of modal structures in inhomogeneous optical waveguides (J. Xia, A. K. Jordan, and J. A. Kong), *Journal of Optical Society of America, A*, Vol. 9, No. 5, 1992.

Electromagnetic radiation from a VLSI package and heatskin configuration (S. Y. Poh, C. F. Lee, K. Li, R. T. Shin, and J. A. Kong), submitted to *IEEE 1991 International Symposium on Electromagnetic Compatibility*, Hyatt Cherry Hill, Cherry Hill, NJ, Au-

gust 13 – 15, 393 – 398, 1991.

A hydrid method of the calculation of resistance and inductance of transmission lines with arbitrary cross section (M. J. Tsuk and J. A. Kong), *IEEE Transactions on Microwave Theory and Techniques*, Vol. 39, No. 8, 1338-1347, 1991.

Analysis of diffraction from chiral gratings (S. H. Yueh and J. A. Kong), *Journal of Electromagnetic Waves and Applications,* Vol. 5, No. 7, 701-714, 1991.

Current distribution, resistance, and inductance for superconducting strip transmission lines (D. M. Sheen, S. M. Ali, D. E. Oates, R. S. Withers, and J. A. Kong), *IEEE Trans. on Applied Superconductivity,* Vol. 1, No. 2, 108–115, June, 1991.

Dyadic Green's functions in a planar stratified, arbitrarily magnetized linear plasma (T. M. Habashy, S. M. Ali, J. A. Kong, and M. D. Grossi), *Radio Science,* Vol. 26, No. 3, 701–716, May – June, 1991.

Electromagnetic calculation of soft x-ray diffraction from 01.μm-scale gold structures (M. L. Schatenburg, K. Li, R. T. Shin, J. A. Kong, D. B. Olster, and H. I. Smith), *Journal of Vacuum Science and Technology* as part of the proceedings of the 35th International Symposium on Electron, Ion, and Photon Beams (paper E84), Seattle, Washington, 1-8, May 28–31, 1991.

Modelling of lossy microstrip lines with finite thickness (J. F. Kiang, S. M. Ali and J. A. Kong), *Progress in Electromagnetics Research*, No. 4, 85-116, Elsevier Publishing Company, 1991.

Input impedance of a probe-fed stacked circular microstrip antenna (A. Tulintseff, S. Ali, and J. A. Kong) *IEEE Transactions on Antennas and Propagation*, Vol. 39, No. 3, 381–390, March 1991.

The propagation characteristics of signal lines with crossing strips in multilayered anisotropic media (C. M. Lam, S. M. Ali, and J. A. Kong), *Journal of Electromagnetic Waves and Application*, Vol. 4, No. 10, 1005–1021, 1990.

Coupled Noise Analysis for Adjacent Vias in Multilayered Digital Circuits

Q. Gu, M.A. Tassoudji, S.Y. Poh, R.T. Shin, J.A. Kong
Research Laboratory of Electronics
Massachusetts Institute of Technology
Cambridge, MA 02139

In high-speed digital circuits, high frequency phenomena affects the characteristics of the interconnections. Physical discontinuities or nonuniformities in the connections may cause severe reflections when they can no longer be considered as conducting wires, but behave as transmission lines and/or waveguides. In multilayered digital circuits, vias constitute one of the most commonly-used class of interconnects.

Vias are not good carriers of high-speed signals. They cause signal distortion and reflections as well as severe degradation in the high frequency components. The analysis and modeling of a single via and some quasi-static or quasi-TEM analyses of single via configurations have been carried out previously. To date, the analysis of coupled noise between adjacent vias has received very little attention. The major reasons include the complexity of multi-via structures and the difficulty of modeling and analyzing them accurately over a broad frequency range.

The electromagnetic coupling between two adjacent vias in a multilayered integrated circuit is analyzed by means of equivalent magnetic frill array models incorporated with the even- and odd-mode approach. Closed-form expressions for the coupled noise on the passive via are derived. The coupling responses in the frequency domain and crosstalk waveforms in the time domain for some multilayered via structures are calculated based on these formulas. A 4-layer experimental model is constructed and measurements are taken for the transmission, reflection, and coupling responses. The measurements show good agreement with the calculated results over a frequency range of up to 18 GHz.

Electromagnetic Radiation from Modules-on-Backplane Configurations in Computer Systems

K. Li, M. A. Tassoudji, S. Y. Poh, R. T. Shin, and J. A. Kong
Research Laboratory of Electronics
Massachusetts Institute of Technology
Cambridge, MA 02139

High frequency digital signals associated with computers and communications equipment have the potential for electromagnetic interference (EMI). The need for compliance with the radiated emissions limits established by FCC and other regulatory agencies for such equipment have led to increased interest in understanding and minimizing EM radiation. As clock speeds increase beyond 100 MHz and edge-rates fall into the sub-nanosecond range, the EMC engineer is faced with FCC tests for frequencies beyond 1 GHz and the prospect of increased energy for frequencies in the hundreds of megahertz range.

The modules-on-backplane configuration is a common assembly scheme for computers. Embedded in these modules and backplane are reference planes which could be as large as tens of centimeters. The reference planes configuration is of interest because the resonant frequencies begin in the low hundreds of megahertz, given typical dimensions. The voltage levels on such reference planes are subject to noise fluctuations (reference noise) originating from disturbances such as inductive discontinuities at connector pins. The increase in power requirements and in the number of simultaneous switching circuits is likely to result in stronger noise sources. A simplified model is used to analyze the modules-on-backplane configuration. Conducting planes model the modules and the backplane. A generator, which is positioned at the module and backplane interface, models the inductive voltage, as a noise source, developed across the module-backplane connector.

The *finite-difference time-domain* (FD-TD) technique, which is based on the discretization of the Maxwell's equations, is employed in this analysis. Nodal electric and magnetic fields are computed on a rectangular grid within a computational domain subject to appropriate boundary and initial conditions. An absorbing boundary condition is enforced on the outer boundary of the computational domain and approximately simulates unbounded space. In the implementation of the FD-TD technique, the areas of concern addressed include the modeling of the excitation as a coaxial line probe and the use of Prony's method to obtain late time responses of the fields for highly resonant configurations. Radiation impedances are obtained from the voltages and currents on the probe and radiation patterns are calculated using Huygens' principle.

Experimental verification is made on physical structures compatible with simulation models. The focus is on correlating computed resonant frequencies and radiation impedances with those deduced from S-parameter measurements taken on a network analyzer. Radiation impedances as functions of frequency are presented for various configurations. Such variations include changing the number of modules and the dimensions and spacings of modules and backplane and the addition of conducting panels to model the shielding or enclosure environment.

This study provides basic information pertaining to the acceptability of noise levels in the interconnect environment for EMI-related considerations. Through the examination of a variety of configurations it will also affect system-level packaging and assembly decisions.

Analyses of Single and coupled Dielectric Rib Waveguides and Discontinuities using the Finite-Difference Time-Domain Method

Alex Mou, Y. Eric Yang, Jin A. Kong
Department of Electrical Engineering and Computer Science
and Research Laboratory of Electronics
Massachusetts Institute of Technology
Cambridge, MA 02139

Millimeter and submillimeter transmission structures are dominated by dielectric waveguides. At these frequency bands, conventional microstrip transmission structures such as microstrip line, coplanar line, slot line and finline all suffer from severe ohmic and radiation losses. Analytical techniques for studying dielectric waveguide structures include the full-wave integral equation formulations (both spectral and spatial domain) and the finite-difference time-domain (FDTD) method. Compared to the integral equation methods, the FDTD method is more straightforward to formulate and provides an alternative path to analyze both time and frequency domain response in the presence of complex structures such as discontinuities.

In this paper, electromagnetic pulse propagation in single and coupled dielectric rib waveguide embedded in a three-layer stratified dielectric medium is simulated and analyzed using the FDTD technique. Time domain transient response of a modulated gaussian pulse is observed in the simulation. We first examine pulse dispersion, attenuation and coupling characteristics for the transmission line structure. Results are found to be in good agreement with those obtained from integral equation methods. We also extend the study to an optical rib waveguide with a bend discontinuity. The FDTD simulation is used to predict the electromagnetic leakage attributed to the discontinuity.

One of the problems facing the FDTD technique for the dielectric waveguide problem is the proper absorbing boundary condition. Existing boundary conditions such as the Mur, Enquist-Majda condition work best when wave incident angle is normal to the boundary, which is generally not the case for dielectric waveguides. A comparison between different conditions will also be presented

Electromagnetic Fields in Metallic Enclosures Lined with Resistive Material

M. A. Tassoudji, K. Li, R. T. Shin, J. A. Kong
Research Laboratory of Electronics
Massachusetts Institute of Technology
Cambridge, MA 02139

M. J. Tsuk
Technology Development and Architecture
Digital Equipment Corporation
Maynard, MA 01754

The use of equipment enclosures to shield against emissions and external energy is a common practice. Efforts range from metal impregnated plastics to thick steel panels incorporating waveguide design in air vents. The choice of complexity depends on system performance and application. The question has often been raised as to whether high field intensities within such enclosures will affect equipment performance. Clearly this is increasingly pertinent in cases of heavy shielding where resonator-like structures with high quality factors (Q) result. Moreover, in these cases, any energy leakage may be highly frequency selective with substantial associated field strength.

The primary motivation for studying such structures is that computers are now operating at faster speeds and consuming more power resulting in significantly increased levels of power at higher frequencies. Also typical metallic enclosure configurations have dimensions which are electrically resonant at frequencies in the hundreds of megahertz range.

This paper focuses on the use of resistive material within the enclosure walls for absorbing some of the contained RF energy, thereby avoiding high Q enclosures and reducing the likelihood of significant field buildup within the enclosure. The energy leakage from perforations on the walls is also being considered. The radiation properties of these structures are observed by varying the number, size and position of the holes in the enclosure.

The finite-difference time-domain (FD-TD) technique is used in analyzing this problem and the metrics are total radiated power and field patterns within the enclosure. The excitation sources are line current source for the two-dimensional models and dipoles for the three-dimensional cases. A Gaussian amplitude is assumed in order to obtain multi-frequency characteristics and to exhibit the resonance properties of the model. In addition to the radiated power through the apertures, the power absorbed in the resistive material is also calculated.

Analysis of Nonuniform Multiconductor Transmission Line Systems – Wave Transmission Matrix Method

Q. Gu, M. A. Tassoudji, and Y. Yuan

Department of Electrical Engineering and Computer Science

and

Research Laboratory of Electronics

Massachusetts Institute of Technology

Cambridge, MA 02139

Abstract

In this paper a new method based on the wave transmission matrix is presented to deal with nonuniform multiconductor line system. This method has not only the ability of handling nonuniformity, but also the advantage of handling nonlinearity efficiently. The wave transmission matrix is employed to characterize the multiconductor transmission lines and the telegrapher equations, therefore, can easily be turned into algebraic equations. The nonuniform transmission line is treated as many small segments of uniform transmission lines connected in cascade. The formulation for this method is described in detail. Calculation approaches are discussed. Numerical results are presented and comparison of them with previous work confirms the validity of the method.

I. Introduction

In very large scale integrated digital circuits and systems, multiconductor transmission lines are commonly used as signal interconnections between chips, chip carriers, circuit boards, or subsystems. As the operating speed of the circuits and the systems increases, the behavior of the multiconductor transmission lines employed as high speed signal carriers will have significant impact on the performance of the circuits or the systems. A multiconductor transmission line usually consists of cylindrical and/or strip conductors embedded in an inhomogeneous medium and one or several of the conductors serving as the ground. Inhomogeneous transmission lines can not support pure TEM waves but quasi-TEM waves at low frequencies. Even if the medium is homogeneous, at higher frequencies due to the conducting loss and higher order mode propagation, the lines are not TEM in nature. Since a rigorous analysis of a multiconductor transmission line is very involved, the analyses in most of previous works and in the following sections are based on the quasi-TEM approximation. In fact, we have seen that this is a very good approximation when the transverse dimensions of the line are small as compared with the operating wavelength [1-11]. In addition to simplifying the analysis of the multiconductor lines, the quasi-TEM approximation is also desired for handling the line terminations which are usually described by circuit quantities (voltages and currents) rather than by the more general field quantities [12]. As the frequency of operation gets higher, the modes start to deviate from the quasi-TEM modes and one must analyze the problem with rigorous full-wave approach [13-15].

The general approach on the analysis of the multiconductor line is as follows: utilizing the electromagnetic field theory to characterize the multiconductor line by developing transmission line parameter matrices, such as the capacitance, inductance, resistance and conductance matrices per unit length of the line, and to establish a mathematical model, i.e., a set of equations governing the behavior of the line system;

and then using preferable method, for example the modal analysis, to solve the equations analytically and/or numerically and to obtain the system responses in the time and frequency domains through corresponding boundary conditions. Here, we shall emphasize the method of analyzing the responses of the multiconductor transmission line in the frequency domain and assume that the parameter matrices of the line are available (refer to [16-21].

When the dominant mode in the multiconductor transmission lines is quasi-TEM, the mathematical model which fully describes the line systems in the time domain or in the frequency domain is the well known telegrapher equations (or refer to as transmission line equations). For uniform multiconductor transmission lines, the corresponding telegrapher equations are most commonly solved by using the so-called modal analysis in the time domain [1-7] or in the frequency domain [7-11]. However, for a lossy or frequency-dependent line, usually the modal analysis in the frequency domain will be used because in this case N different quasi-TEM modes propagating on a transmission line with N signal conductors and one ground conductor can be defined in the frequency domain only. In the modal analyses, the kernel of the approach is to decouple the telegrapher equations by utilizing the method of characteristics, and then based on given boundary conditions the problem can be solved in a variety of ways, for example, by solving directly [3,6-7], or by network analysis methods [10]. Other approaches for the analysis of the multiconductor transmission line are the equivalent circuit model techniques [22-23], and matrix parameter methods (Green's function methods) [24-29]. The modal analyses can not directly deal with nonuniform multiconductor line problems, but incorporating with other techniques, such as the perturbation method, iteration method, or the numerical method, it is still possible to use the modal analysis in the time domain for some nonuniform systems [3,5,30]. However, the more efficient

methods for handling the nonuniform transmission lines are the network matrix parameter methods [24-29] in the frequency domain and the spectral method [31] in the time domain.

We shall present a new method based on the wave transmission matrix to deal with the nonuniform multiconductor line system in this paper. This method has not only the ability of handling nonuniformity, but also the advantage of handling nonlinearity in the terminations efficiently. The wave transmission matrix is employed to characterize the multiconductor transmission lines and the telegrapher equations, therefore, can easily be turned into algebraic equations. The nonuniform transmission line is treated as many small segments of uniform transmission lines connected in cascade. The boundary conditions are formulated with linear loads in spectral domain and with nonlinear loads in time domain.

The details of this method will be described in Sections II. The treatment of the boundary conditions including nonlinear terminations will be discussed in Section III. Calculation approach and numerical results will be presented in Sections IV and V.

II. Analysis and Formulation

The general system configuration under consideration is shown in figure 1. The system consists of multiconductor interconnection lines terminated with linear/nonlinear loads. In this section, we use the wave transmission matrix to characterize the multiconductor transmission lines. The boundary condition or termination will be considered in next section.

For lossy multiconductor transmission lines, the telegrapher equations in the frequency domain can be expressed as

$$\frac{\partial}{\partial z}\begin{bmatrix}\mathbf{V}\\ \mathbf{I}\end{bmatrix} = -\begin{bmatrix}\mathbf{0} & \mathbf{Z}\\ \mathbf{Y} & \mathbf{0}\end{bmatrix}\begin{bmatrix}\mathbf{V}\\ \mathbf{I}\end{bmatrix} \tag{1}$$

where $\mathbf{V}$ and $\mathbf{I}$ are the N dimensional voltage and current vectors on the N transmission lines, and $\mathbf{Z}$ and $\mathbf{Y}$ denote the $N \times N$ impedance and admittance matrices per unit length, respectively. The matrices $\mathbf{Z}$ and $\mathbf{Y}$ are symmetric. For uniform multiconductor lines, they are related to $N \times N$ resistance ($\mathbf{R}$), inductance ($\mathbf{L}$), conductance ($\mathbf{G}$), and capacitance ($\mathbf{C}$) real matrices per unit length as follows:

$$\mathbf{Z} = \mathbf{R} + j\omega\mathbf{L} \tag{2}$$

$$\mathbf{Y} = \mathbf{G} + j\omega\mathbf{C} \tag{3}$$

Now, we define a forward-going and a backward-going voltage wave vectors, $\mathbf{V}^+$ and $\mathbf{V}^-$, as

$$\mathbf{V}^{\pm} = \mathbf{V} \pm \mathbf{Z}_0\mathbf{I} \tag{4}$$

or the voltage $\mathbf{V}$ and the current $\mathbf{I}$ as

$$\mathbf{V} = \frac{1}{2}(\mathbf{V}^+ + \mathbf{V}^-) \tag{5}$$

$$\mathbf{I} = \frac{1}{2}\mathbf{Z}_0^{-1}(\mathbf{V}^+ - \mathbf{V}^-) \tag{6}$$

where $\mathbf{Z}_0$ is defined in any of the following equivalent forms:

$$\mathbf{Z}_0 = (\mathbf{ZY})^{1/2}\mathbf{Y}^{-1} = (\mathbf{ZY})^{-1/2}\mathbf{Z} \tag{7}$$

Substituting (5) and (6) into (1) and after some mathematical manipulation, we obtain the wave transmission equations

$$\frac{\partial}{\partial z}\begin{bmatrix}\mathbf{V}^+ \\ \mathbf{V}^-\end{bmatrix} = \frac{1}{2}\begin{bmatrix}-(\mathbf{Z}\mathbf{Z}_0^{-1} + \mathbf{Z}_0\mathbf{Y}) & (\mathbf{Z}\mathbf{Z}_0^{-1} - \mathbf{Z}_0\mathbf{Y}) \\ -(\mathbf{Z}\mathbf{Z}_0^{-1} - \mathbf{Z}_0\mathbf{Y}) & (\mathbf{Z}\mathbf{Z}_0^{-1} + \mathbf{Z}_0\mathbf{Y})\end{bmatrix}\begin{bmatrix}\mathbf{V}^+ \\ \mathbf{V}^-\end{bmatrix} \tag{8}$$

It is easy to prove that the diagonal elements of the 2×2 partitioned matrix on the right-hand side of (8) are $-(\mathbf{ZY})^{1/2}$ and $(\mathbf{ZY})^{1/2}$, and the off diagonal elementary matrices equal zero. Equation (8) can be rewritten as

$$\frac{\partial}{\partial z}\begin{bmatrix}\mathbf{V}^+ \\ \mathbf{V}^-\end{bmatrix} = \begin{bmatrix}-(\mathbf{ZY})^{1/2} & \mathbf{0} \\ \mathbf{0} & (\mathbf{ZY})^{1/2}\end{bmatrix}\begin{bmatrix}\mathbf{V}^+ \\ \mathbf{V}^-\end{bmatrix} \tag{9}$$

where 0 denotes a matrix with all the elements being 0.

From (9), we can see that the forward-going wave vector $\mathbf{V}^+$ and the backward-going wave vector $\mathbf{V}^-$ are decoupled from each other. This is only true for uniform multiconductor transmission lines. There exists coupling between these two wave vectors for nonuniform transmission lines, because the travelling wave in either direction is continuously reflected by the nonuniformity of the lines along the propagation direction.

The equations in (9) are first order derivative matrix equations, it is obvious that their solutions have the forms:

$$\mathbf{V}^+(z) = \mathbf{V}_0^+ exp(-\mathbf{K}z) \tag{10}$$

$$\mathbf{V}^-(z) = \mathbf{V}_0^- exp(\mathbf{K}z) \tag{11}$$

where $\mathbf{V}_0^{\pm}$ are constant vectors to be determined by boundary conditions of the lines, and $\mathbf{K}$ is the propagation constant matrix of the line,

$$\mathbf{K} = \sqrt{\mathbf{ZY}} \tag{12}$$

As we know that the voltage wave vectors at any two positions, z_1 and z_2, on the transmission line are related through a wave transmission matrix, the vectors at z, $\mathbf{V}^{\pm}(z)$, therefore, can be obtained from the wave vectors at $z = 0$, $\mathbf{V}^{\pm}(0)$, in terms of the following expression

$$\begin{bmatrix} \mathbf{V}^+(z) \\ \mathbf{V}^-(z) \end{bmatrix} = \begin{bmatrix} \mathbf{A}_{11}(z) & \mathbf{A}_{12}(z) \\ \mathbf{A}_{21}(z) & \mathbf{A}_{22}(z) \end{bmatrix} \begin{bmatrix} \mathbf{V}^+(0) \\ \mathbf{V}^-(0) \end{bmatrix} \tag{13}$$

where $[\mathbf{A}_{ij}]$ is the wave transmission matrix of the transmission line segment between z and 0. The elementary matrices $\mathbf{A}_{ij}\,(i,j = 1,2)$ in the wave transmission matrix can be easily obtained by utilizing (10) and (11), and they are, respectively:

$$\mathbf{A}_{11}(z) = exp(-\mathbf{K}z) = 1 - \mathbf{K}\frac{z}{1!} + (\mathbf{K})^2\frac{z^2}{2!} - (\mathbf{K})^3\frac{z^3}{3!} + \cdots + (-1)^k(\mathbf{K})^k\frac{z^k}{k!} + \cdots \tag{14a}$$

$$\mathbf{A}_{12}(z) = \mathbf{A}_{21}(z) = \mathbf{0} \tag{14b}$$

and

$$\mathbf{A}_{22}(z) = exp(\mathbf{K}z) = \mathbf{1} + \mathbf{K}\frac{z}{1!} + (\mathbf{K})^2\frac{z^2}{2!} + (\mathbf{K})^3\frac{z^3}{3!} + \cdots + (\mathbf{K})^k\frac{z^k}{k!} + \cdots \tag{14c}$$

where $\mathbf{1}$ is the unit matrix. The features of the wave transmission matrix are very similar to the chain parameter matrix, those identities given in [24] are also suitable for the wave transmission matrix.

For a nonuniform multiconductor transmission line, we can approximate it as many small uniform line segments with different characteristic impedance matrix $\mathbf{Z}_{0k}$ $(k = 1, 2, \ldots, m)$ connected in cascade. The wave transmission matrix $[\mathbf{A}_{ij}]$ for the whole multiconductor line can be expressed in product of sub-wave-transmission-matrices $[\mathbf{A}_{k,ij}]$ characterizing each small line segment, and impedance transition submatrices $[\mathbf{T}_{k,ij}]$,

$$\begin{bmatrix} \mathbf{A}_{11} & \mathbf{A}_{12} \\ \mathbf{A}_{21} & \mathbf{A}_{22} \end{bmatrix} = \begin{bmatrix} \mathbf{A}_{m,11} & \mathbf{A}_{m,12} \\ \mathbf{A}_{m,21} & \mathbf{A}_{m,22} \end{bmatrix} \prod_{k=m-1}^{1} \left(\begin{bmatrix} \mathbf{T}_{k,11} & \mathbf{T}_{k,12} \\ \mathbf{T}_{k,21} & \mathbf{T}_{k,22} \end{bmatrix} \begin{bmatrix} \mathbf{A}_{k,11} & \mathbf{A}_{k,12} \\ \mathbf{A}_{k,21} & \mathbf{A}_{k,22} \end{bmatrix} \right) \tag{15}$$

where $\mathbf{A}_{k,ij}$ $(i, j = 1, 2)$ have the same forms as (14), and they are:

$$\mathbf{A}_{k,11} = exp(-\mathbf{K}_k \Delta\ell_k) = \sum_{p=0}^{\infty} \frac{(-1)^p}{p!} (\mathbf{K}_k \Delta\ell_k)^p \tag{16a}$$

$$\mathbf{A}_{k,12} = \mathbf{A}_{k,21} = \mathbf{0} \tag{16b}$$

and

$$\mathbf{A}_{k,22} = exp(\mathbf{K}_k \Delta\ell_k) = \sum_{p=0}^{\infty} \frac{1}{p!} (\mathbf{K}_k \Delta\ell_k)^p \tag{16c}$$

where $\Delta\ell_k$ is the length of the kth uniform segment at $z = z_k$, and $\mathbf{K}_k$ is the propagation constant matrix of the kth segment and it can be expressed by the per unit length impedance and admittance matrices of the kth segment, $\mathbf{Z}_k$ and $\mathbf{Y}_k$, as

$$\mathbf{K}_k = \sqrt{\mathbf{Z}_k \mathbf{Y}_k}. \tag{17}$$

In (15), the elementary matrices $\mathbf{T}_{k,ij}$ in the impedance transition submatrices have the following forms:

$$\mathbf{T}_{k,11} = \mathbf{T}_{k,22} = \frac{1}{2}(\mathbf{Z}_{0,k} + \mathbf{Z}_{0,k+1})\mathbf{Z}_{0,k}^{-1} \tag{18}$$

and

$$\mathbf{T}_{k,12} = \mathbf{T}_{k,21} = \frac{1}{2}(\mathbf{Z}_{0,k} - \mathbf{Z}_{0,k+1})\mathbf{Z}_{0,k}^{-1} \tag{19}$$

where $\mathbf{Z}_{0,k}\,(k = 1, 2, \ldots, m)$ is the characteristic impedance matrix of the kth uniform segment.

Comparing (15) with (13), we can see that in the nonuniform case the off diagonal elementary matrices $\mathbf{A}_{12}$ and $\mathbf{A}_{21}$ are not zero matrices. This means that there exists coupling between the forward-going and backward-going voltage waves, $\mathbf{V}^+$ and $\mathbf{V}^-$ due to reflection caused by the nonuniformities along the line. The coupling between forward- and backward-going waves will be weak if the nonuniformities are small.

In reality, uniform or nonuniform multiconductor transmission lines are usually terminated with linear and/or nonlinear loads. The solution for the multiconductor transmission line systems must be related to boundary conditions of the systems. The approaches for treating different boundary conditions will be described in the next section.

III. Boundary Conditions

In the previous section the multiconductor transmission lines were characterized by the wave transmission matrix A. In order to analyze the total response of the system, the terminations or boundary conditions need to be considered. In this section we formulate the boundary conditions with linear loads in spectral domain and with nonlinear loads in time domain.

We assume Thevenin equivalent voltage sources and impedances for the linear terminations of the multiconductor transmission line system of length ℓ as shown in Figure 1. Thus the boundary conditions are:

$$\mathbf{V}(0) = \mathbf{E}_S - \mathbf{Z}_S\mathbf{I}(0) \tag{20}$$

and

$$\mathbf{V}(\ell) = \mathbf{E}_L + \mathbf{Z}_L\mathbf{I}(\ell) \tag{21}$$

where $\mathbf{E}_S$ and $\mathbf{E}_L$ denote excitation voltage vectors at $z = 0$ and $z = \ell$, respectively, and $\mathbf{Z}_S$ and $\mathbf{Z}_L$ are $N \times N$ diagonal source and load impedance matrices at the corresponding ends.

For linear terminations, we can determine the boundary values of the forward- and backward-going voltage wave vectors from (20) and (21) using (5), (6) and (13). The final expressions of the boundary values $\mathbf{V}^+(0)$ and $\mathbf{V}^-(\ell)$ are:

$$\begin{aligned}\mathbf{V}^+(0) = &[1 - \Gamma_S\mathbf{A}_{22}^{-1}\mathbf{A}_{21} - \Gamma_S\mathbf{A}_{22}^{-1}(1 + \Gamma_L\mathbf{A}_{12}\mathbf{A}_{22}^{-1})^{-1}\Gamma_L\mathbf{Z}_{0m}\mathbf{Z}_{01}^{-1}\mathbf{A}_{22}^{-1}]^{-1} \\ &[\mathbf{T}_S\mathbf{E}_S - \Gamma_S\mathbf{A}_{22}^{-1}(1 + \Gamma_L\mathbf{A}_{12}\mathbf{A}_{22}^{-1})^{-1}\mathbf{T}_L\mathbf{E}_L)]\end{aligned} \tag{22}$$

and

$$\begin{aligned}\mathbf{V}^-(\ell) = &[1 + \Gamma_L\mathbf{A}_{22}^{-1}\mathbf{A}_{12} - \Gamma_L\mathbf{Z}_{0m}\mathbf{Z}_{01}^{-1}\mathbf{A}_{22}^{-1}(1 - \Gamma_S\mathbf{A}_{22}^{-1}\mathbf{A}_{21})^{-1}\Gamma_S\mathbf{A}_{22}^{-1}]^{-1} \\ &[\mathbf{T}_L\mathbf{E}_L - \Gamma_L\mathbf{Z}_{0m}\mathbf{Z}_{01}^{-1}\mathbf{A}_{22}^{-1}(1 - \Gamma_S\mathbf{A}_{22}^{-1}\mathbf{A}_{21})^{-1}\mathbf{T}_S\mathbf{E}_S)]\end{aligned} \tag{23}$$

where $\Gamma_{S,L}$ and $\mathbf{T}_{S,L}$ are

$$\Gamma_{S,L} = (1 + \mathbf{Z}_{S,L}\mathbf{Z}_{01,0m}^{-1})^{-1}(1 - \mathbf{Z}_{S,L}\mathbf{Z}_0^{-1}) \tag{24}$$

and

$$\mathbf{T}_{S,L} = 2(1 + \mathbf{Z}_{S,L}\mathbf{Z}_{01,0m}^{-1})^{-1} \tag{25}$$

where $\mathbf{Z}_{01}$ and $\mathbf{Z}_{0m}$ are the characteristic impedance matrices of the first and the last line segments. When deriving (22) and (23), the following identity has been used.

$$\mathbf{A}_{11}\mathbf{A}_{22} - \mathbf{A}_{12}\mathbf{A}_{22}^{-1}\mathbf{A}_{21}\mathbf{A}_{22} = \mathbf{Z}_{0m}\mathbf{Z}_{01}^{-1} \tag{26}$$

The voltage wave vectors at any point z on the line can be obtained from (13) and the boundary values (22) and (23), and they are:

$$\begin{bmatrix} \mathbf{V}^+(z) \\ \mathbf{V}^-(z) \end{bmatrix} = \begin{bmatrix} \mathbf{A}_{11}(z) & \mathbf{A}_{12}(z) \\ \mathbf{A}_{21}(z) & \mathbf{A}_{22}(z) \end{bmatrix} \begin{bmatrix} \mathbf{1} & \mathbf{0} \\ -\mathbf{A}_{22}^{-1}(\ell)\mathbf{A}_{21}^{-1}(\ell) & \mathbf{A}_{22}^{-1}(\ell) \end{bmatrix} \begin{bmatrix} \mathbf{V}^+(0) \\ \mathbf{V}^-(\ell) \end{bmatrix} \tag{27}$$

where matrix $[\mathbf{A}_{ij}(z)]$ is

$$\begin{bmatrix} \mathbf{A}_{11}(z) & \mathbf{A}_{12}(z) \\ \mathbf{A}_{21}(z) & \mathbf{A}_{22}(z) \end{bmatrix} = \begin{bmatrix} \mathbf{A}_{m_1,11} & \mathbf{A}_{m_1,12} \\ \mathbf{A}_{m_1,21} & \mathbf{A}_{m_1,22} \end{bmatrix} \Bigg|_{m_1=z/\Delta\ell} \cdot \prod_{k=m_1-1}^{1} \left(\begin{bmatrix} \mathbf{T}_{k,11} & \mathbf{T}_{k,12} \\ \mathbf{T}_{k,21} & \mathbf{T}_{k,22} \end{bmatrix} \begin{bmatrix} \mathbf{A}_{k,11} & \mathbf{A}_{k,12} \\ \mathbf{A}_{k,21} & \mathbf{A}_{k,22} \end{bmatrix} \right) \tag{28}$$

The results derived here are in frequency domain and should be performed for each frequency separately. The time response of the voltages can be obtained using Fourier transform.

For nonlinear terminations of the multiconductor transmission lines, the analysis of boundary conditions utilizes the incident wave, $\mathbf{V}^{inc}$, and reflected wave, $\mathbf{V}^{ref}$, which are related by the scattering wave matrix S.

$$\mathbf{V}^{ref} = \mathbf{S}\mathbf{V}^{inc} \tag{29}$$

or in terms of elementary scattering matrices as,

$$\begin{bmatrix} \mathbf{V}^{ref}(0) \\ \mathbf{V}^{ref}(l) \end{bmatrix} = \begin{bmatrix} \mathbf{S}_{11} & \mathbf{S}_{12} \\ \mathbf{S}_{21} & \mathbf{S}_{22} \end{bmatrix} \begin{bmatrix} \mathbf{V}^{inc}(0) \\ \mathbf{V}^{inc}(l) \end{bmatrix} \tag{30}$$

where $V^{inc}(0)$ and $V^{inc}(l)$ are the incident voltage wave vectors at $z = 0$ and $z = l$, and $V^{ref}(0)$ and $V^{ref}(l)$ are the reflected voltage wave vectors at $z = 0$ and $z = l$. The $\mathbf{S}_{ij}$ are related to the elementary wave transmission matrices $\mathbf{A}_{ij}$ as follows

$$\mathbf{S}_{11} = -\mathbf{A}_{22}^{-1}\mathbf{A}_{21}$$

$$\mathbf{S}_{12} = \mathbf{A}_{22}^{-1}$$

$$\mathbf{S}_{21} = \mathbf{A}_{11} - \mathbf{A}_{12}\mathbf{A}_{22}^{-1}\mathbf{A}_{21}$$

$$\mathbf{S}_{22} = \mathbf{A}_{12}\mathbf{A}_{22}^{-1}$$

The relation between the reflected and incident voltage vector in time domain can be written as

$$\mathbf{v}^{ref} = \mathbf{h} * \mathbf{v}^{inc} \tag{31}$$

where h is the inverse Fourier transform of the scattering matrix S and asterisk denotes convolution with respect to time.

Consider the N nonuniform transmission lines, where each line is terminated by a voltage source and a load. Using the relationship of the incident and reflected wave with the current and voltage, the following expressions can be obtained,

$$\mathbf{v}^{inc} = \mathbf{v}' + \mathbf{e} - \mathbf{z} * \mathbf{i} \tag{32}$$

$$\mathbf{v}^{ref} = \mathbf{v}' + \mathbf{e} + \mathbf{z} * \mathbf{i} \tag{33}$$

where $\mathbf{v}'$ is the voltage vector across the loads, e is the voltage source vector, i is the current vector and each of its elements is a function of the corresponding element of $\mathbf{v}'$. The matrix z is the inverse Fourier transform of the diagonal impedance matrix characterizing the terminal impedance lines. The first N diagonal elements of z correspond to the impedances of the terminal lines connected to the first segments of the transmission lines and the latter N elements correspond to the impedances of the terminal lines connected to the last segments.

To solve the equations (31)-(33) numerically, we discretize the time variable and convert the convolution integrals into summation. After some manipulation, we obtain

$$\mathbf{v'}_k = -\mathbf{e}_k + [1 - \mathbf{h}_0]^{-1} \left\{ \sum_{m=0}^{k-1} \mathbf{h}_{k-m} \mathbf{v}_m^{inc} - [1 + \mathbf{h}_0] \sum_{m=0}^{k} \mathbf{z}_{k-m} \mathbf{i}_m \right\} \tag{34}$$

In the above equation, the subscripts denote the discretized time step, for instant $\mathbf{v'}_k = \mathbf{v}'(k\Delta t)$, where Δt is the time step. Equation (34) is a set of nonlinear algebraic equations, which can be solved by means of numerical techniques, such as the Newton Raphson technique. The incident voltage used in equation (34) can be obtained from

$$\mathbf{v}_k^{inc} = \mathbf{v'}_k + \mathbf{e}_k - \sum_{m=0}^{k} \mathbf{z}_{k-m} \mathbf{i}_m \tag{35}$$

The above formulation would also work for linear loads for which the current will be the ratio of v' to the load impedance.

IV. Computational Consideration

The major part in the numerical implementation of this method consists of various matrix operations and manipulations, including calculation of matrix functions such as square-root and exponential functions.

In the calculation of wave transmission matrix, the square-root manipulation of a matrix is involved as shown in (12). A formal approach to carry out the square-root of a matrix is to transform the matrix into a diagonalized matrix, i.e., to use the characteristics method. Define a matrix $\mathbf{X}$ to be the square-root of $\mathbf{ZY}$, then we have

$$\mathbf{ZY} = \mathbf{XX} \tag{36}$$

Assuming that the eigenvalue and eigenvector of $\mathbf{ZY}$ are β_i^2 and $\mathbf{D}_i$, respectively, they must have the following relationship

$$\mathbf{D}^{-1}\mathbf{ZYD} = \mathrm{diag}[\beta_i^2] \tag{37}$$

where $\mathbf{D}$ is a matrix consisting of the eigenvectors $\mathbf{D}_i$, i.e., $\mathbf{D} = [\mathbf{D}_1, \mathbf{D}_2, \ldots, \mathbf{D}_N]$. Substituting (36) into (37), we obtain

$$\mathrm{diag}[\beta_i^2] = \mathbf{D}^{-1}\mathbf{ZYD} = \mathbf{D}^{-1}\mathbf{XDD}^{-1}\mathbf{XD} \tag{38}$$

From above, $\sqrt{\mathbf{ZY}}$ is obtained as

$$\mathbf{X} = \sqrt{\mathbf{ZY}} = \mathbf{D}\,\mathrm{diag}[\beta_i]\mathbf{D}^{-1} \tag{39}$$

In general, a matrix function can be defined and calculated by the following formula

$$f(\mathbf{W}) = \mathbf{D}\,\mathrm{diag}[f(\lambda_1), f(\lambda_2), \ldots, f(\lambda_N)]\mathbf{D}^{-1} \tag{40}$$

where $f(\cdot)$ denotes a function, such as square root and/or exponential function, and λ_i is the eigenvalue and $\mathbf{D}$ is the matrix consisting of eigenvectors of matrix $\mathbf{W}$.

The elementary matrices $\mathbf{A}_{ij}$ $(i,j = 1,2)$ defined by (16a-c) can be calculated directly by the series expansion. The matrix series are absolutely convergent and their convergence rates depend upon the magnitude of eigenvalues of $\sqrt{\mathbf{Z}_k\mathbf{Y}_k}$, $\beta_{k,i}(i = 1,2,\ldots,N)$, and the length $\Delta\ell_k$ of the line segments. The smaller the product $|\beta_{k,i}|\Delta\ell_k$, the higher the convergence rate. Therefore, in order to obtain high convergence rate we need to divide the uniform/nonuniform line into large number of short segments, which is computationally expensive. The exponential matrix functions can also be calculated using equation (40), as in the calculation of square-root function. However the latter requires the calculation of the eigenvectors of the matrix, a procedure very time consuming numerically.

An alternative approach to calculate the elementary matrices is to make use of the following Sylvester's formula [32]. If a $N \times N$ matrix $\mathbf{W}$ has N distinct eigenvalues, a function of matrix $\mathbf{W}$ can then be calculated by

$$f(\mathbf{W}) = \sum_{r=1}^{N} f(\lambda_r)\mathbf{Z}_r \tag{41}$$

where λ_r are eigenvalues of matrix $\mathbf{W}$, and $\mathbf{Z}_r$ are $N \times N$ matrices given by

$$\mathbf{Z}_r = \prod_{\substack{i=1 \\ i\neq r}}^{N} \frac{\mathbf{W} - \lambda_i\mathbf{1}}{\lambda_r - \lambda_i} \tag{42}$$

The matrices $\mathbf{Z}_r$ satisfy the following relations:

$$\sum_{r=1}^{N} \mathbf{Z}_r = \mathbf{1}, \quad \text{and} \quad \mathbf{Z}_r\mathbf{Z}_s = \mathbf{0} \quad (r \neq s) \tag{43}$$

The approach using equation (41) avoids the calculation of the eigenvector and, since it uses exact formula as (40) instead of series expansion, it also avoids the problem of convergence. Therefore it is numerically much more simpler and faster. Moreover, by

using (41) in the calculation of the elementary matrix $\mathbf{A}_{ij}$, the manipulation of square-root and exponential of matrix $\sqrt{\mathbf{Z}_k\mathbf{Y}_k}$ can be combined and accomplished in one procedure. For the cases of coupled microstrip lines, the eigenvalues which correspond to coupled modes of the structures are always non-degenerate due to the coupling effect. In our numerical implementation, both approaches have been used, if the eigenvalues of the matrix product $\mathbf{ZY}$ are distinct. Same results are obtained, while the Sylvester's formula significantly reduces the computation time.

To validate the present method and its numerical implementation, here we consider a pair of symmetric nonuniformly coupled lines. For this case, the elementary matrices in (16) and (17) are 2×2 and they can be calculated analytically. Assuming the pair of nonuniform transmission lines have the following impedance matrix $\mathbf{Z}$ and admittance matrix $\mathbf{Y}$:

$$\mathbf{Z} = \begin{bmatrix} R(z) & 0 \\ 0 & R(z) \end{bmatrix} + j\omega \begin{bmatrix} L(z) & L_m(z) \\ L_m(z) & L(z) \end{bmatrix} \tag{44a}$$

and

$$\mathbf{Y} = \begin{bmatrix} G(z) & 0 \\ 0 & G(z) \end{bmatrix} + j\omega \begin{bmatrix} C(z) & C_m(z) \\ C_m(z) & C(z) \end{bmatrix} \tag{44b}$$

Then the square root of $\mathbf{ZY}$ can be obtained by the following expression

$$\mathbf{K} = \sqrt{\mathbf{ZY}} = \frac{1}{2} \begin{bmatrix} \gamma_+ + \gamma_- & \gamma_+ - \gamma_- \\ \gamma_+ - \gamma_- & \gamma_+ + \gamma_- \end{bmatrix} \tag{45}$$

where γ_+ and γ_- are the eigenvalues of $\mathbf{K}$ given by

$$\gamma_+ = \sqrt{[R(z) + j\omega(L(z) + L_m(z))][G(z) + j\omega(C(z) + C_m(z))]} \tag{46a}$$

and

$$\gamma_- = \sqrt{[R(z) + j\omega(L(z) - L_m(z))][G(z) + j\omega(C(z) - C_m(z))]} \tag{46b}$$

The exponential function in (16a,c) are given by the following expression

$$exp(-\mathbf{K}\Delta\ell) = \frac{1}{2} \begin{bmatrix} exp(\gamma_+\Delta\ell) + exp(\gamma_-\Delta\ell) & exp(\gamma_+\Delta\ell) - exp(\gamma_-\Delta\ell) \\ exp(\gamma_+\Delta\ell) - exp(\gamma_-\Delta\ell) & exp(\gamma_+\Delta\ell) + exp(\gamma_-\Delta\ell) \end{bmatrix} \tag{47}$$

The characteristic impedance matrix Z_0 will be

$$\begin{aligned}\mathbf{Z_0} &= \sqrt{\mathbf{ZY}}\mathbf{Y}^{-1} \\ &= \frac{1}{2}\begin{bmatrix} \frac{G+j\omega C}{\Delta C}(\gamma_+ + \gamma_-) - \frac{j\omega C_m}{\Delta C}(\gamma_+ - \gamma_-) & \frac{G+j\omega C}{\Delta C}(\gamma_+ - \gamma_-) - \frac{j\omega C_m}{\Delta C}(\gamma_+ + \gamma_-) \\ \frac{G+j\omega C}{\Delta C}(\gamma_+ - \gamma_-) - \frac{j\omega C_m}{\Delta C}(\gamma_+ + \gamma_-) & \frac{G+j\omega C}{\Delta C}(\gamma_+ + \gamma_-) - \frac{j\omega C_m}{\Delta C}(\gamma_+ - \gamma_-) \end{bmatrix}\end{aligned} \tag{48}$$

where

$$\Delta C = (G + j\omega C)^2 + \omega^2 C_m^2.$$

For this example, we use the same parameters as that in Fig. 8 in [5]. The total length of the line is 1cm. The elements of matrices Z and Y in (44) are:

$$\begin{aligned} L(z) &= 5.73(1 - k_L(z)) \qquad \text{(nH/cm)} \\ L_m(z) &= k_L(z)L(z) \qquad \text{(nH/cm)} \\ C(z) &= 1.81(1 + k_C(z)) \qquad \text{(pF/cm)} \\ C_m(z) &= -k_C(z)C(z) \qquad \text{(pF/cm)} \\ k_C(z) &= 0.2 - 0.05[1 - cos(2\pi z)] \\ k_L(z) &= 0.2 \\ R(z) &= G(z) = 0 \end{aligned} \tag{49}$$

A pulse source with amplitude 10 Volts, both rise time and fall time of 10 ps, and duration 20 ps is imposed on one end of the lines and all the ends are terminated with 50 Ω load. The time waveforms of the voltage at each end are given in Fig. 2. These results compares very well with those of [5], especially for the near end and far end coupling noises. The numerical calculations of the matrix are compared with analytical results when possible and very good agreement is found, therefore verified the numerical codes.

V. Numerical Examples

In this section, several examples of nonuniform multiconductor microstrip lines with linear or nonlinear terminations are considered. In the analysis of any transmission line system, we need first to construct the impedance matrix **Z** and admittance matrix **Y**, as defined in (2) and (3) by resistance (**R**), inductance (**L**), conductance (**G**), and capacitance (**C**) matrices. Many methods have been developed to calculate the impedance and admittance of microstrip lines. However, the formulation developed in the previous sections does not depend on the ways those parameter matrices are calculated. Moreover, by introducing different effects in the parameter matrices, the same effects can be incorporated into the system signal responses. For example, if the inductance and capacitance are calculated as frequency dependent, then the dispersion can be included, if the skin effects are considered in the calculation of resistance and conductance, the overall losses as a function of frequency can be determined. In the following examples, we calculated the inductance and capacitance in a way similar to that of [35]. The resistance and conductance are calculated by the strip cross section and the metal conductivity. The elementary matrices $\mathbf{A}_{ij}$ are computed by utilizing (41) (Sylvester's formula) for the uniform/nonuniform regions.

As first example, the nonuniform coupled interconnection, given as example 5 in [31], is analyzed. A ramp function incidence with a rise time 100 ps and an amplitude 1 volt is applied on the active line. At beginning, we employed a frequency bandwidth from DC to 100 GHz, and obtained the time waveforms on the active and passive lines as shown in Fig. 3(a) and 3(b), respectively. Comparing them with those results presented in [31] and [33], we found that our waveforms are sharper than theirs. As we use less frequency bandwidth, such as from DC to 15 Ghz, the resulting waveforms are smoother as shown in Fig. 4(a) and 4(b), and they are very similar to those given in [31] and [33]. In the calculation, we use 80 small uniform segments with equal length to approximate the nonuniform region of this coupled interconnection. The CPU time is 3

minutes and 50 seconds on DEC Station 3100 for the 100 GHz case with 500 frequency points.

As discussed in Section III, multiple line system with nonlinear terminations can be analyzed efficiently in terms of scattering matrix and the corresponding impulse responses in time domain. As the second example, we consider the case of two uniformly coupled lines with nonlinear terminations. In order to check our results, we used the same L,C, R and G parameter matrices and nonlinear load as that given in [25]. Fig. 5(a) gives the near-end and far-end voltage responses on the active line, and Fig. 5(b) gives those on the parasitic line. Our results match very well with that of [25]. This further confirms that our method is efficient and valid for solving multiconductor line with nonlinear termination.

In the following example, we analyze a more complicated three nonuniform microstrip line structure with both linear and nonlinear terminations. The transmission line system and the cross section of the microstrip are depicted in Fig. 6. The thickness of the metal strip is assumed to be $T = 5\mu/m$. The surface resistance of the metal strip is $R = 30m\Omega/square$. In our calculation, the 1cm long nonuniform microstrip is divided into 50 segments for computing the elementary matrices. The incidence voltage is a step function with an amplitude of 1 volt. First, we calculated the linear load case where all ends are terminated with 50 Ω resistors. Fig. 7(a) shows the near-ends response voltages and Fig. 7(b) shows the far-end responses. These results compare very well with that given in [34], even though the L,C, R and G matrices are calculated differently and the strip thickness is not given in [34].

Next, we calculated the case where the active line far-end termination was replaced by a nonlinear load , but the rest were kept the same. The nonlinear load is a diode with nonlinear characteristics $i = I_s(e^{V/V_T} - 1)$, where $I_s = 1\text{mA}$ and $V_T = 25\text{mV}$. In Fig. 8(a) and 8(b), the voltage waveforms on the far and near end terminals of the three lines are shown. Comparing Fig. 8 with Fig. 7, we can see that the nonlinear

load not only varies the waveform at port 4 on the active line, but also changes the waveforms at the other ports.

VI. Conclusions

A new method based on the wave transmission matrix to deal with nonuniform multiconductor transmission lines has been developed. One of the advantages of this method is the flexibility of handling a variety of nonuniform multiline structures, because in most cases it is possible to approximately deal with a nonuniform multiline as small segments of uniform multiline connected in cascade, and the total wave transmission matrix will be the multiplication of all the submatrices representing each small uniform segment. The other virtue is that uniform or weak nonuniform multilines will have diagonalized wave transmission matrices. This method is developed on the variables, forward going and backward going waves, instead of the voltage and current, it is consistent with the method solving nonlinear problems in terms of scattering matrix and the corresponding impulse responses [27,28]. They can be easily incorporated, and then an approach to handle nonuniform multiconductor transmission line with nonlinear termination problems can be achieved. This combination method is very efficient to solve the nonuniform structure with nonlinear termination problems, even if the nonuniform structure is a lossless or very low lossy system. The methods based on the voltage and current variables will have hard time to deal with the very low lossy multiline with nonlinear termination problems.

The examples given in the previous section firmly validate that this method is efficient to deal with nonuniform multilines and is significant to corporate with the method solving nonlinear termination problems. It is possible to extend the combination method for solving more general nonuniform and nonlinear problems.

Acknowledgment

This work was supported by ONR Contract N00014-90-J-1002 and Joint Services Electronics Program under the Contract DAAL03-92-C-0001.

References

[1] F.Y. Chang, "Transient analysis of lossless coupled transmission lines in a non-homogeneous dielectric medium," *IEEE Trans. Microwave Theory Tech.*, vol. MTT-18, pp. 616-626, Sept. 1970.

[2] M.K. Krage and G.I. Haddad, "Characteristics of coupled microstrip transmission lines with inhomogeneous dielectrics," *IEEE Trans. Microwave Theory Tech.*, vol. MTT-20, pp.678-688, Oct. 1972.

[3] Y.C.E. Yang, J.A. Kong, and Q. Gu, "Time-domain perturbational analysis of nonuniformly coupled transmission lines," *IEEE Trans. Microwave Theory Tech.*, vol. MTT-33, pp. 1120-1130, Nov. 1985.

[4] J.E. Schutt-Aine and R. Mittra, "Analysis of pulse propagation in coupled transmission lines," *IEEE Trans. Circuit Syst.*, vol. CAS-32, pp. 1214-1219, Dec. 1985.

[5] Q. Gu, J.A. Kong, and Y.E. Yang, "Time domain analysis of nonuniformly coupled line systems," *J. Electromag. Waves Appl.*, vol. 1, pp. 109-132, 1987.

[6] H. You and M. Soma, "Crosstalk analysis of interconnection lines and packages in high-speed integrated circuits," *IEEE Trans. Circuit Syst.*, vol. CAS-37, pp. 1019-1026, Aug. 1990.

[7] A.R. Djordevic', T.K. Sarkar, and R.F. Harrington, "Time-domain response of multiconductor transmission lines," *Proc. IEEE*, vol. 75, pp743-764, June 1987.

[8] A.J. Groudis and C.S. Chang, "Coupled lossy transmission line characterization and simulation," *IBM J. Res. Develop.*, vol. 25, pp.25-41, Jan. 1981

[9] Q. Gu and J.A. Kong, "Transient analysis of single and coupled lines with capacitively-loaded junctions," *IEEE Trans. Microwave Theory Tech.*, vol. MTT-34, pp. 952-964, Sept. 1986.

[10] J.E. Schutt-Aine and R. Mittra, "Nonlinear transient analysis of coupled transmission lines," *IEEE Trans. Circuit Syst.*, vol. CAS-36, pp. 959-967, July 1989.

[11] J.F. Mao and Z.F. Li, "Analysis of the time response of multiconductor transmission lines with frequency-dependent losses by the method of convolution characteristics," *IEEE Trans. Microwave Theory Tech.*, vol. MTT-40, pp. 637-644, Apr. 1992.

[12] L. Carin and K.J. Wabb, "An equivalent circuit model for terminated hybrid-mode multiconductor transmission lines," *IEEE Trans. Microwave Theory Tech.*, vol. MTT-37, pp. 1784-1793, Nov. 1989.

[13] G. Ghione, I. Maio, and G. Vecchi, "Modeling of multiconductor buses and analysis of crosstalk, propagation delay and pulse distortion in high-speed GaAs logic circuits," *IEEE Trans. Microwave Theory Tech.*, vol. MTT-37, pp. 445-456, Mar. 1989.

[14] J.P. Gilb and C.A. Balanis, "Pulse distortion on multilayer coupled microstrip lines," *IEEE Trans. Microwave Theory Tech.*, vol. MTT-37, pp. 1620-1628, Oct. 1989.

[15] R. Wang and O. Wing, "A circuit model of a system of VLSI interconnects for time response computation," *IEEE Trans. Microwave Theory Tech.*, vol. MTT-39, pp. 688-693, Apr. 1991.

[16] T. Itoh and R. Mittra, "Spectral-domain approach for calculating the dispersion characteristics of microstrip lines," *IEEE Trans. Microwave Theory Tech.*, vol. MTT-21, pp. 496-499, 1973.

[17] C. Wei, R.F. Harrington, J.R. Mautz, and T.K. Sarkar, "Multiconductor transmission lines in multilayered dielectric media," *IEEE Trans. Microwave Theory Tech.*, vol. MTT-32, pp. 439-450, Apr. 1984.

[18] E.G. Farr, C.H. Chan, and R. Mittra, "A frequency-dependent coupled-mode analysis of multiconductor microstrip lines with application to VLSI interconnection problems," *IEEE Trans. Microwave Theory Tech.*, vol. MTT-34, pp.307-310, Feb. 1986.

[19] F. Medina and M. Horno, "Capacitance and inductance matrices for microstrip structures in multilayered anisotropic dielectrics," *IEEE Trans. Microwave Theory Tech.*, vol. MTT-35, pp. 1002-1008, Nov. 1987.

[20] N. Fache and D.D. Zutter, "Rigorous full-wave space-domain solution for dispersive microstrip lines," *IEEE Trans. Microwave Theory Tech.*, vol. MTT- 36, pp. 731-737, Apr. 1988.

[21] F. Olyslager, N. Fache, and D.D. Zutter, "New fast and accurate lines in multilayered media," *IEEE Trans. Microwave Theory Tech.*, vol. MTT-39, pp. 901-909, June 1991.

[22] A.J. Groudis, "Transient analysis of uniform resistive transmission lines in a homogeneous medium," *IBM J. Res. Develop.*, vol. 23, pp. 675-681, Nov. 1979.

[23] F.Y. Chang, "Waveform relaxation analysis of RLCG transmission lines," *IEEE Trans. Circuit Syst.*, vol. CAS-37, pp. 1394-1415, Nov. 1990.

[24] C.R. Paul, "Useful matrix chain parameter identities for the analysis of multiconductor transmission lines," *IEEE Trans. Microwave Theory Tech.*, vol. MTT-23, pp.756-760, Sept. 1975.

[25] A.R. Djordjevic', T.K. Sarkar, and R.F. Harrington, "Analysis of lossy transmission lines with arbitrary nonlinear terminal networks," *IEEE Trans. Microwave Theory Tech.*, vol. MTT-34, pp. 640-666, June 1986.

[26] J.E. Schutt-Aine and R. Mittra, "Scattering parameter transient analysis of transmission lines loaded with nonlinear terminations," *IEEE Trans. Microwave Theory Tech.*, vol. MTT-36, pp. 529-536, Mar. 1988.

[27] Q. Gu, Y.E. Yang, and J.A. Kong, "Transient analysis of frequency-dependent transmission line systems terminated with nonlinear loads," *J. Electromag. Waves appl.*, vol. 3, No. 3, pp. 183-197, 1989.

[28] Q. Gu, D.M. Sheen, and S.M. Ali, "Analysis of transients in frequency-dependent interconnections and planar circuits with nonlinear loads," *IEE Proc. Pt. H*, vol. 139, pp. 38-44, Feb. 1992.

[29] J.F. Mao and Z.F. Li, "Analysis of the time response of nonuniform multiconductor transmission lines with a method of equivalent cascaded network chain," *IEEE Trans. Microwave Theory Tech.*, vol. MTT-40, pp. 948-954, May 1992.

[30] J.E. Adair and G.I. Haddad, "Coupled-mode analysis of non-uniform coupled transmission lines," *IEEE Trans. Microwave Theory Tech.*, vol. MTT-17, pp. 746-752, Oct. 1969.

[31] O.A. Palusinki and A. Lee, "Analysis of transients in nonuniform and uniform multiconductor transmission lines," *IEEE Trans. Microwave Theory Tech.*, vol. MTT-37, pp. 127-138, Jan. 1989.

[32] S. Barnett, *Matrix Method for Engineers and Scientists,* McGRAW-HILL Book Company (UK) Limited, 1979.

[33] G.W. Pan, G.J. Wunsch, and B.K. Gilbert, "Frequency-domain analysis of coupled nonuniform transmission lines using chebyshev pseudo-spatial techniques," *IEEE Trans. Microwave Theory Tech.*, vol. MTT-40, pp. 2025-2033, Nov. 1992.

[34] N. Orhanovic, V.K. Tripathi, and P. Wang, "Time domain simulation of uniform and nonuniform multiconductor lossy lines by the method of characteristics," *1990 IEEE MTT-S Digest*, pp. 1191-1194, June 1990.

[35] W. T. Weeks, "Calculation of coefficients of capacitance of multiconductor transmission lines in the presence of a dielectric interface," *IEEE Trans. Microwave Theory Tech.*, vol. MTT-18, pp. 35-43, Jan. 1970.

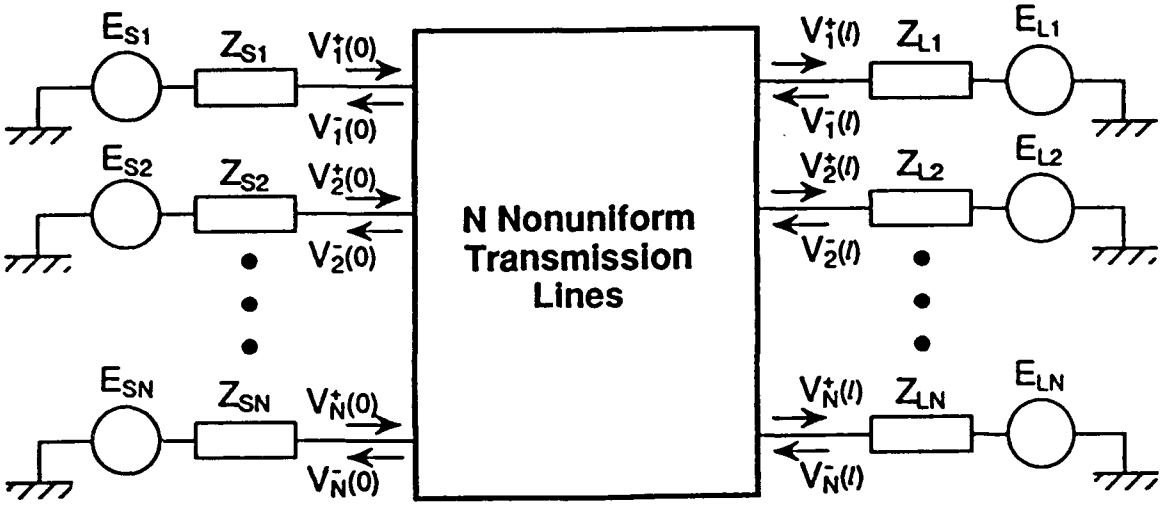
E_{S1}
Z_{S1}
$V_1^+(0)$
$V_1^-(0)$
E_{S2}
Z_{S2}
$V_2^+(0)$
$V_2^-(0)$
E_{SN}
Z_{SN}
$V_N^+(0)$
$V_N^-(0)$
N Nonuniform Transmission Lines
$V_1^+(l)$
Z_{L1}
E_{L1}
$V_1^-(l)$
$V_2^+(l)$
Z_{L2}
E_{L2}
$V_2^-(l)$
$V_N^+(l)$
Z_{LN}
E_{LN}
$V_N^-(l)$

Fig. 1

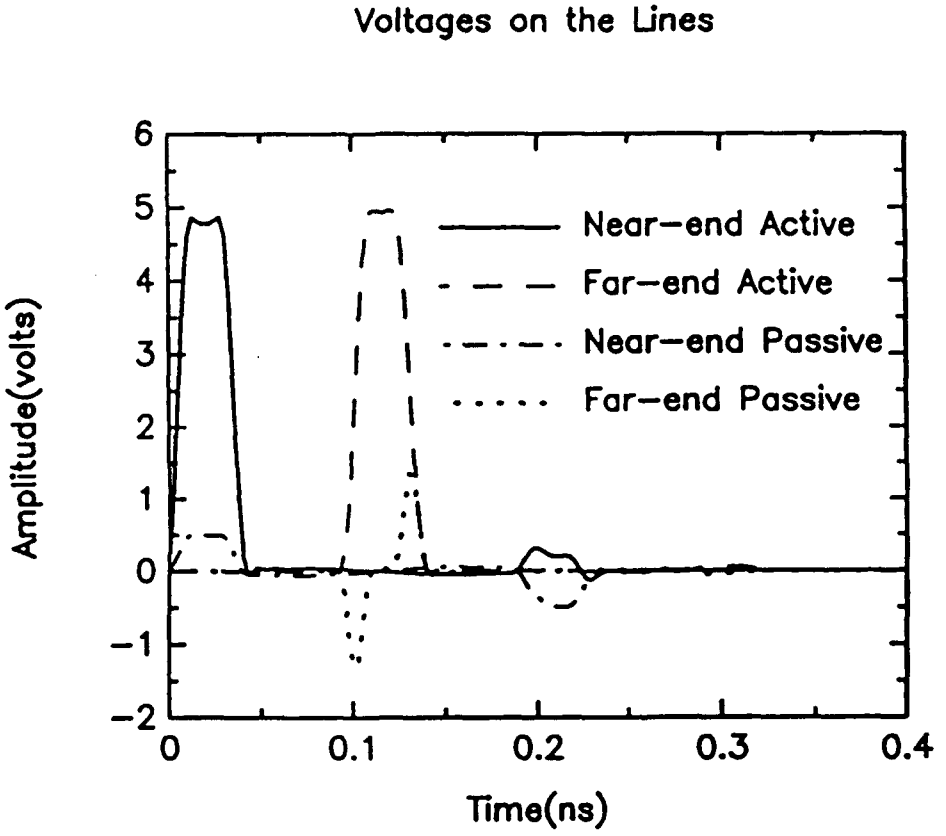
Voltages on the Lines
Amplitude(volts)
Time(ns)
Near–end Active
Far–end Active
Near–end Passive
Far–end Passive
6
5
4
3
2
1
0
−1
−2
0
0.1
0.2
0.3
0.4

Fig. 2

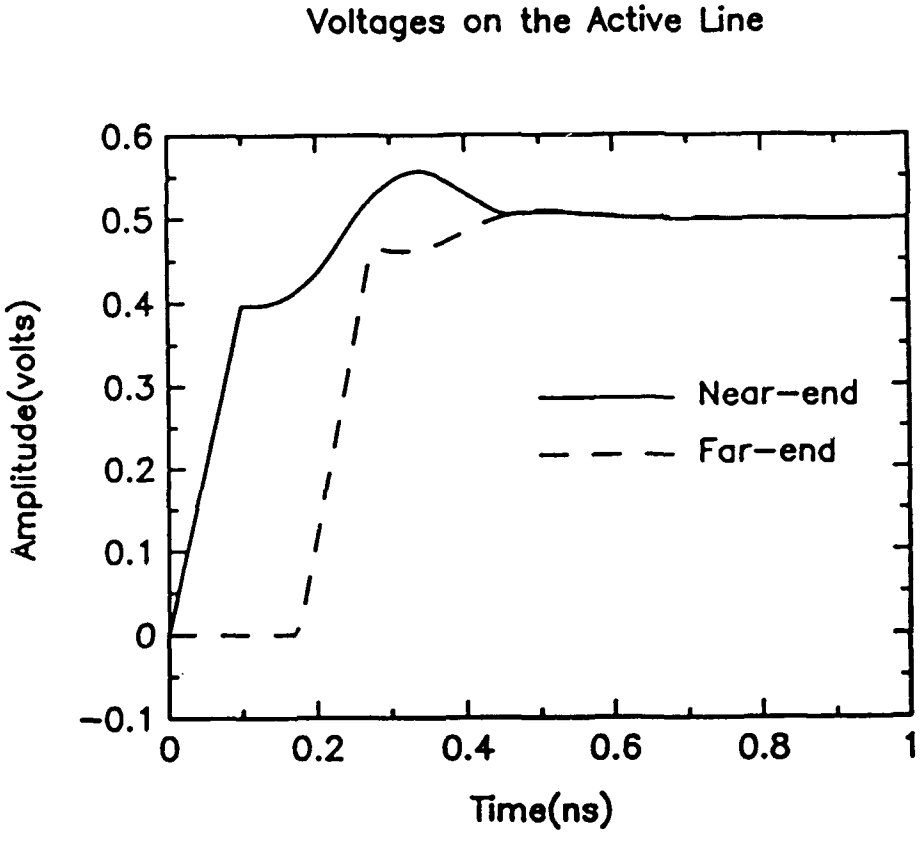

Fig. 3a

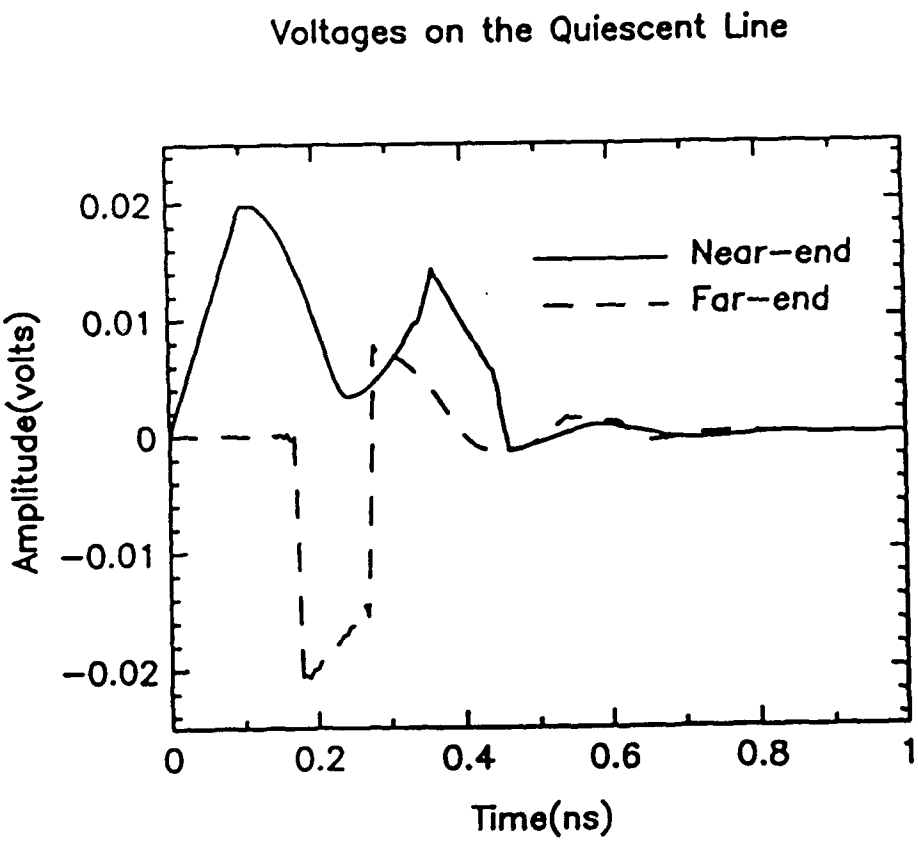

Fig. 3b

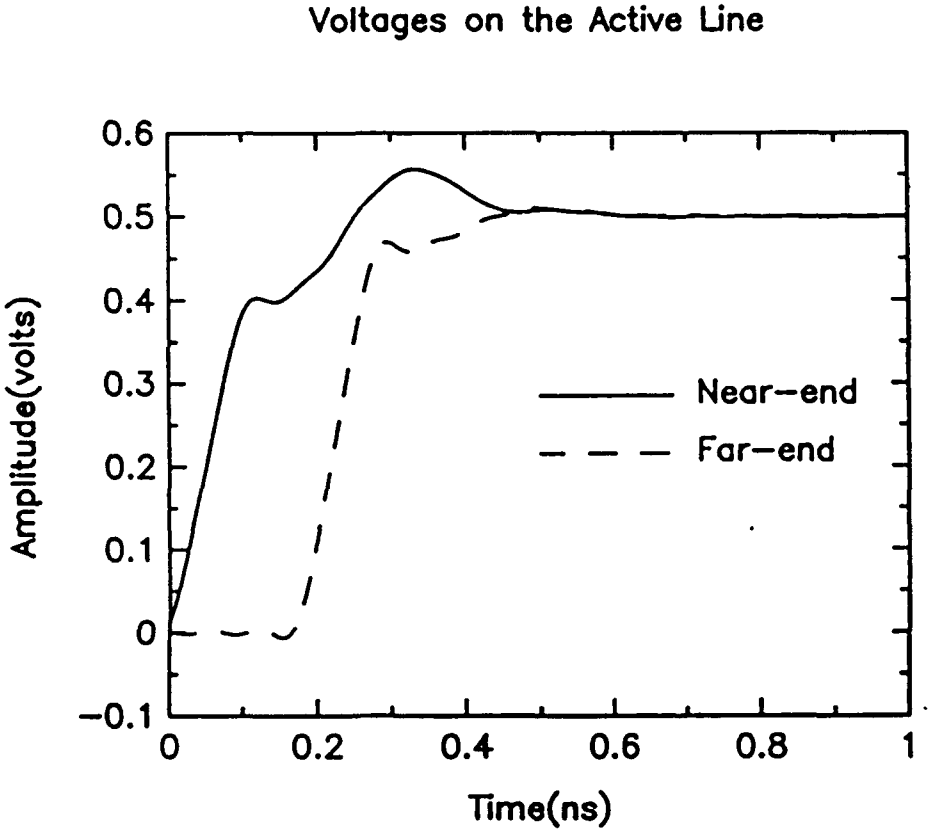

Fig. 4a

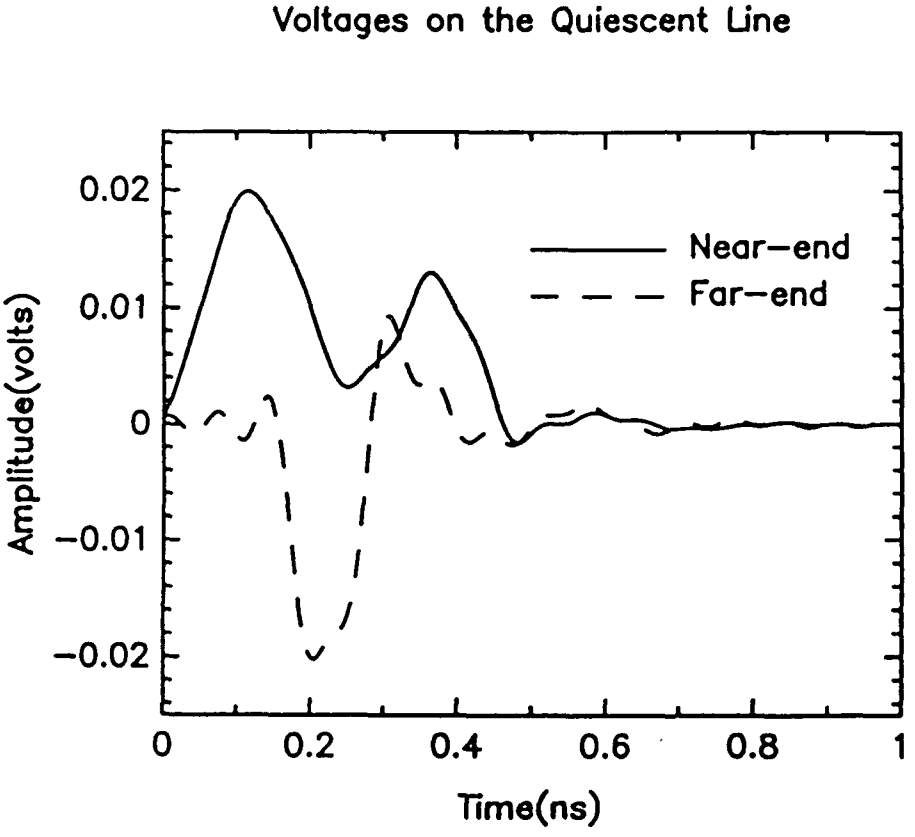
Voltages on the Quiescent Line
0.02
0.01
0
−0.01
−0.02
Amplitude(volts)
Near−end
Far−end
0
0.2
0.4
0.6
0.8
1
Time(ns)

Fig. 4b

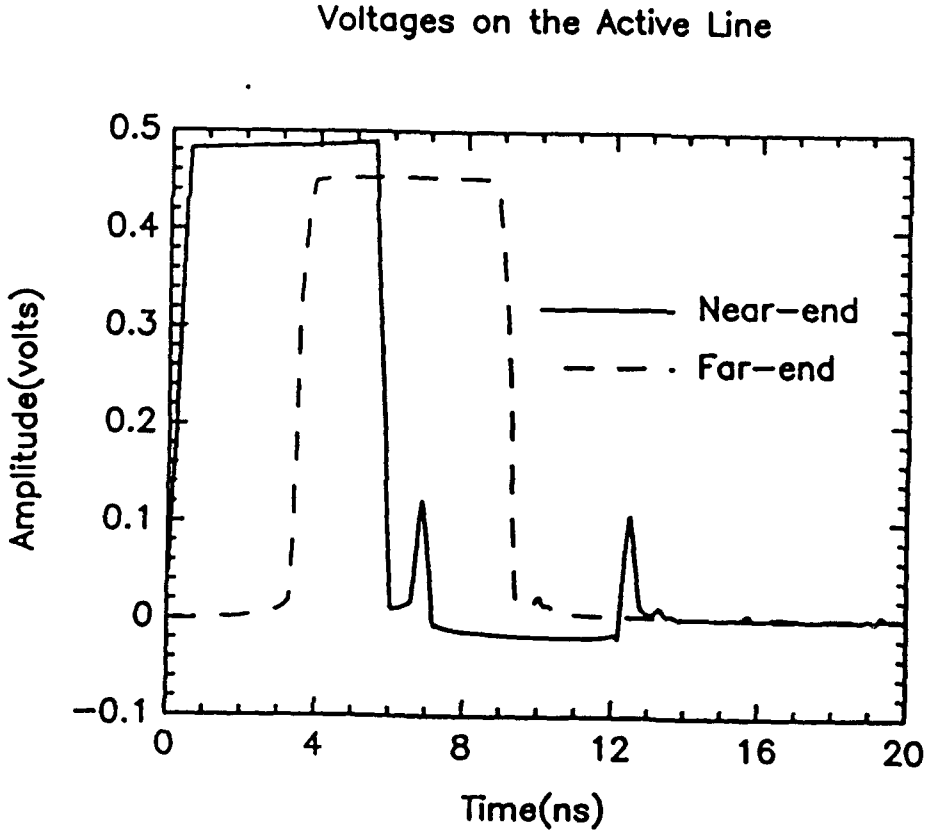
Voltages on the Active Line
0.5
0.4
0.3
0.2
0.1
0
−0.1
Amplitude(volts)
0
4
8
12
16
20
Time(ns)
Near−end
Far−end

Fig. 5a

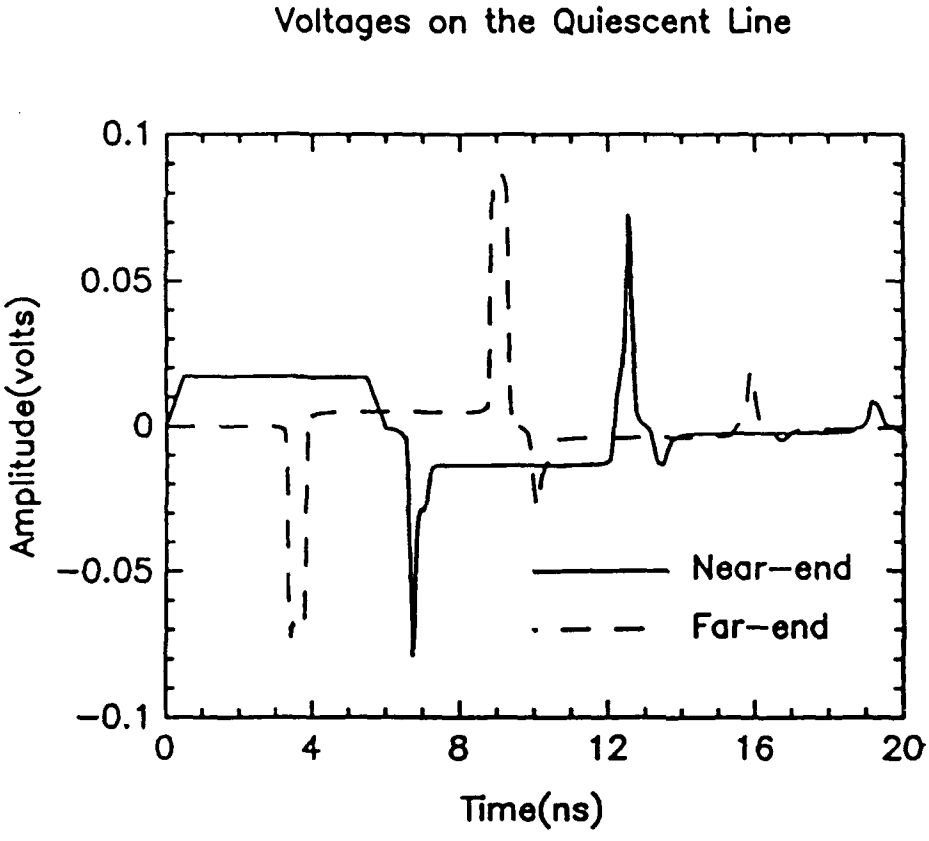
Voltages on the Quiescent Line
0.1
0.05
0
−0.05
−0.1
Amplitude(volts)
0
4
8
12
16
20
Time(ns)
Near−end
Far−end

Fig. 5b

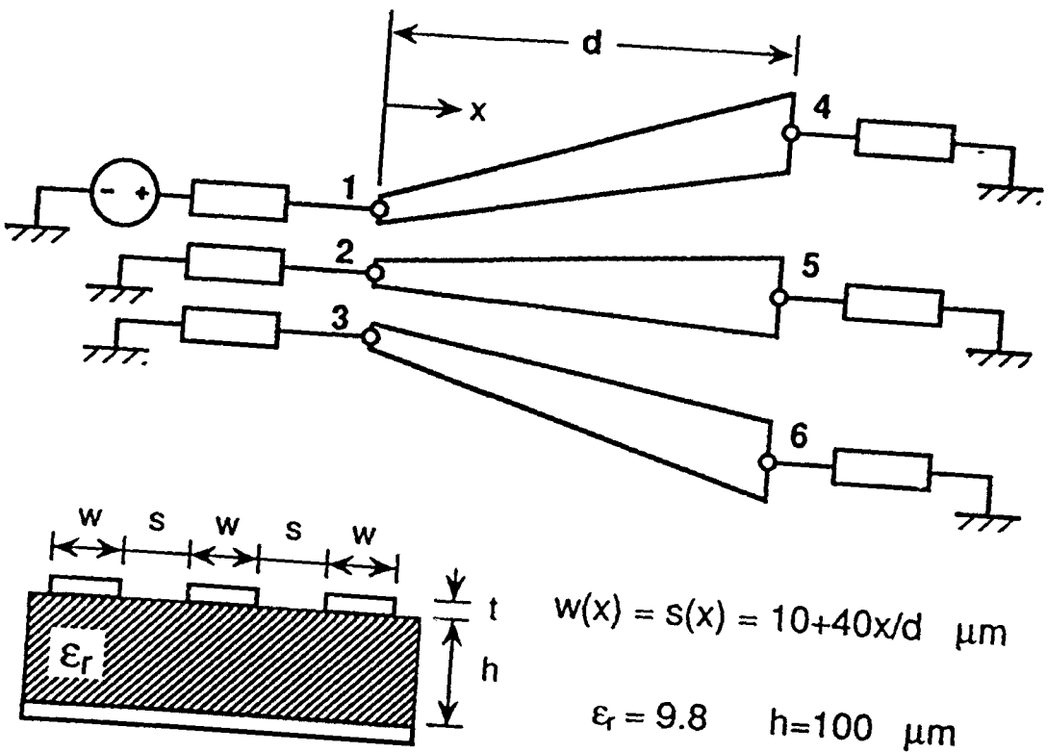
d
x
1
2
3
4
5
6
w
s
w
s
w
t
h
ε_r
w(x) = s(x) = 10+40x/d μm
ε_r = 9.8 h=100 μm

Fig. 6

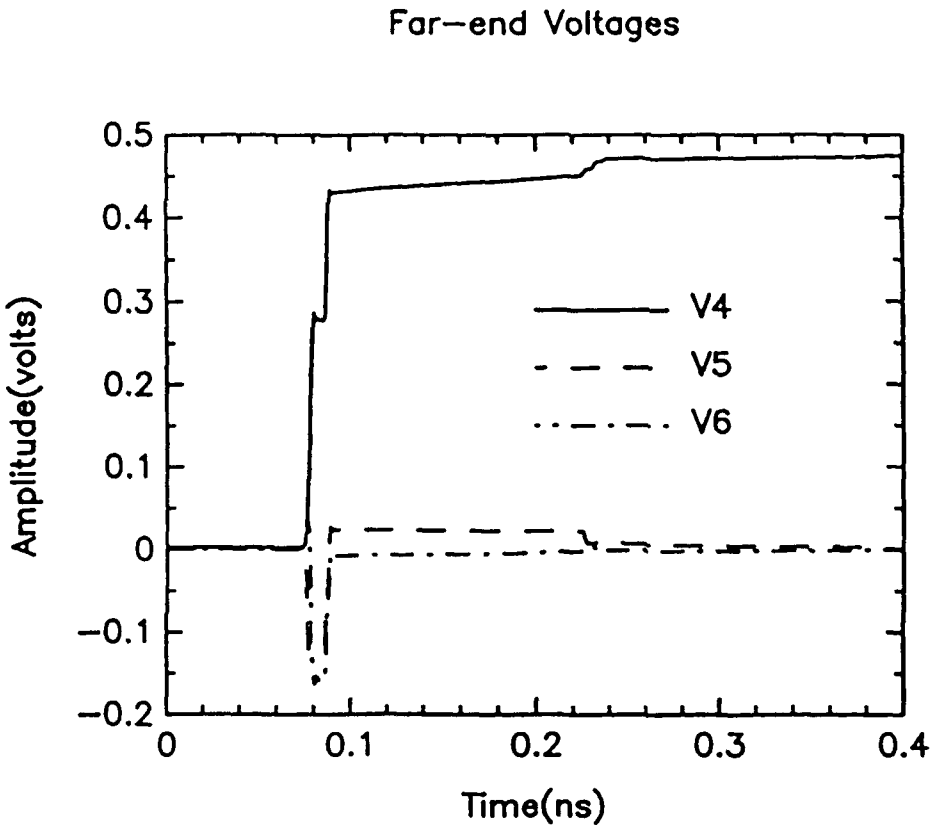
Far-end Voltages
0.5
0.4
0.3
0.2
0.1
0
-0.1
-0.2
Amplitude(volts)
V4
V5
V6
0
0.1
0.2
0.3
0.4
Time(ns)

Fig. 7a

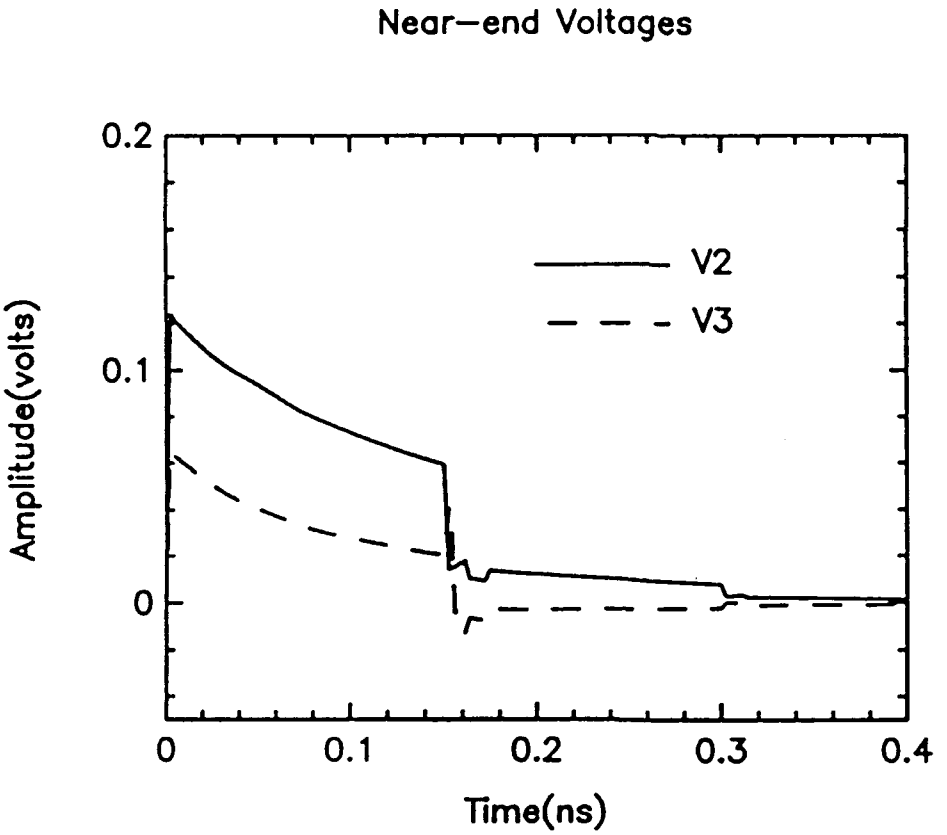
Near–end Voltages
0.2
0.1
0
Amplitude(volts)
V2
V3
0
0.1
0.2
0.3
0.4
Time(ns)

Fig. 7b

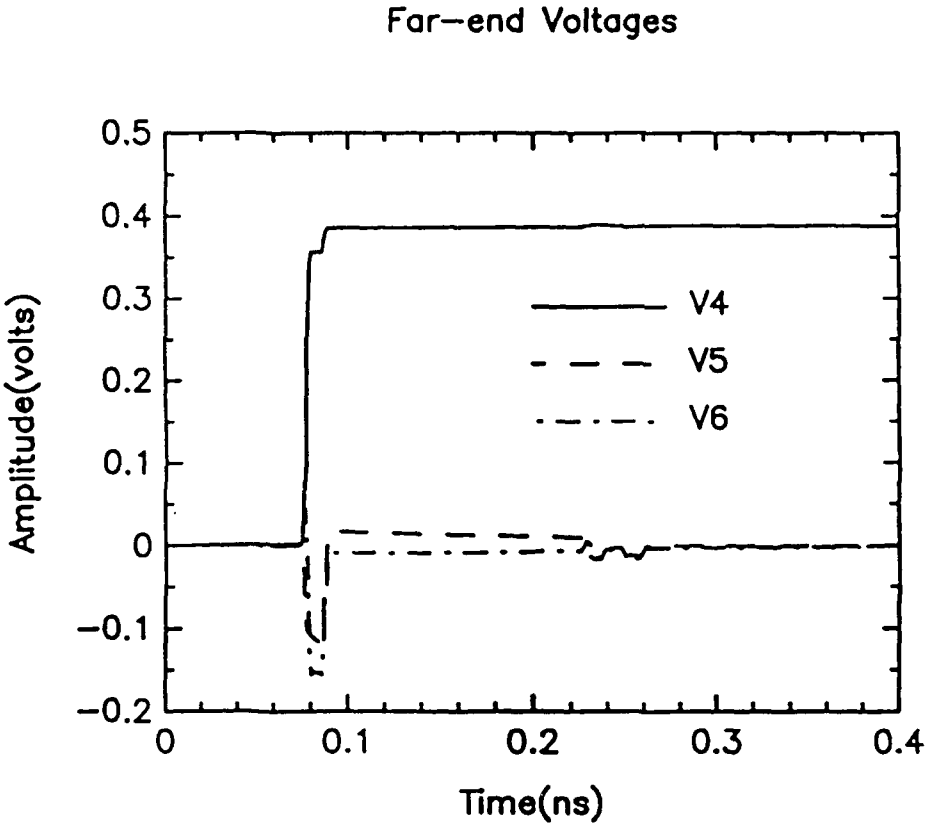
Far-end Voltages
0.5
0.4
0.3
0.2
0.1
0
−0.1
−0.2
Amplitude(volts)
V4
V5
V6
0
0.1
0.2
0.3
0.4
Time(ns)

Fig. 8a

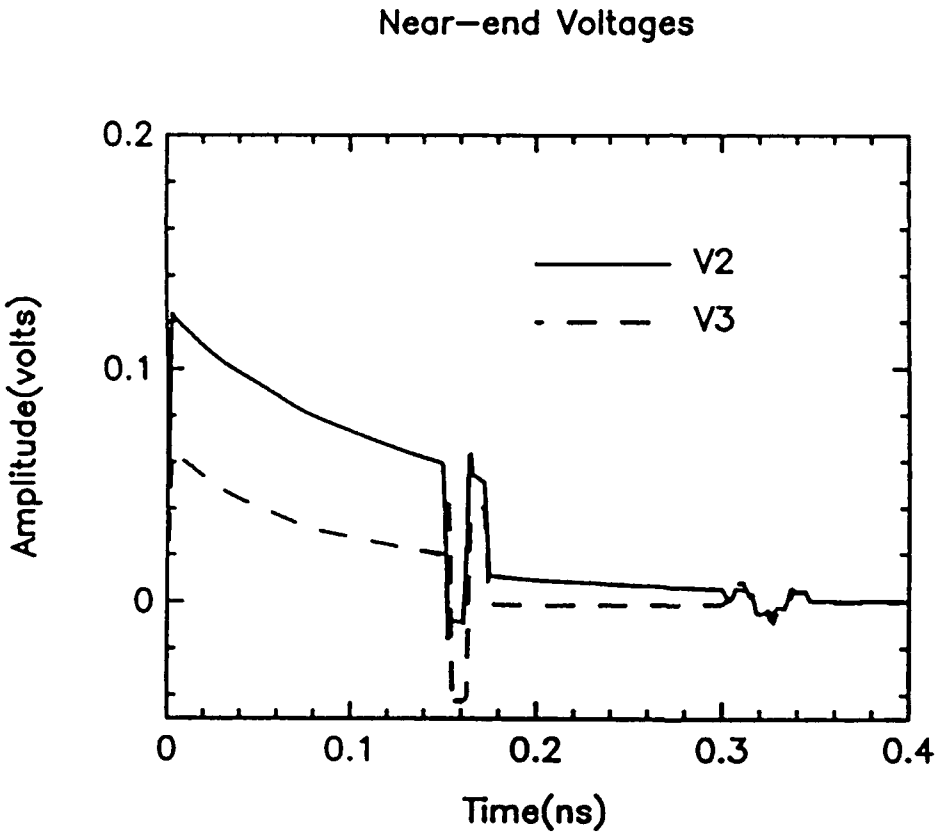

Fig 8b

A Macroscopic Model of Nonlinear Constitutive Relations in Superconductors

Jake J. Xia

Jin A. Kong

Robert T. Shin

Research Laboratory of Electronics

Massachusetts Institute of Technology

Cambridge, MA 02139

Abstract

A macroscopic model is proposed for nonlinear electromagnetic phenomena in superconductors. Nonlinear constitutive relations are derived by modifying the linear London's equations. The superelectron number density as a function of applied macroscopic current density, $n_s(J)$, is derived from a distribution of electron velocities at a certain temperature T. At temperature $T \neq 0$K, the function $n_s(J)$ has a smooth variation near the macroscopic critical current density J_c. Agreement has been found between this $n_s(J,T)$ model and the temperature dependence of n_s in the two-fluid model. The nonlinear conductivities $\sigma_s(J)$ and $\sigma_n(J)$ are obtained from the London's equation with the modified $n_s(J)$ function. Nonlinear resistance $R(I)$, kinetic inductance $L_k(I)$ and surface impedance $Z_s(I)$ in thin wire, slab, and strip geometries are calculated.

I. Introduction

Superconductors have great potential applications in many fields. For example, in microwave integrated circuits, high-Q resonators and microstrips can be made of superconductors with low losses. The discovery of high-Tc superconductors has also made a big impact on modeling of superconductors. Problem of modeling nonlinear electromagnetic properties of a superconductor is of practical importance [1-9]. For example, in application of superconductors to high-Q resonators, fields and currents are very large at resonance and nonlinear effects are inevitable.

In this paper, we use the macroscopic (classical) theory to model nonlinear superconductivity. The constitutive relations which relate electric field $\overline{E}$ and magnetic field $\overline{B}$ to superconducting current density $\overline{J}_s$ will be derived. The model is based on two London equations and the two-fluid model. New problem at hand is to incorporate the nonlinear effects into the constitutive relations. Application of the nonlinear constitutive relations will provide new methods for studying nonlinear effects in superconductors.

There are different types of nonlinearity in superconductors. One type of nonlinearity is displayed in polycrystalline superconductors where granular currents are involved [1,2]. The granular nonlinearity occurs when the current I is above I_c (here I_c is the threshold current of the grain junctions). It is similar to a p-n junction's exponential $I-V$ relation. It is also found in type II superconductors that the vortex motion in the mixing state (between the superconducting and the normal states) can cause a nonlinear $V-I$ relation when current density J is slightly greater than the critical current density J_c [3]. The granular or vortex nonlinearity will not be discussed in this paper.

Another type of nonlinearity is intrinsic for all superconductors. This is due to the de-

pendence of superelectron number density n_s on the applied current density J. This nonlinearity is more general. There have been few papers in literature directly addressing this nonlinearity problem. In this paper we will focus on this intrinsic nonlinearity.

It is necessary to point out that this paper is based on macroscopic theory with certain hypotheses. The authors do not intend to propose a rigorous microscopic theory to explain the nonlinear superconductivity. The purpose of this paper is to provide engineers with a material-independent macroscopic model for nonlinearities in superconductors. The model will be based on macroscopic parameters. The model is intended to achieve the following: (1) explain the nonlinear voltage-current ($V - I$) relations and the dependence of inductances on currents ($L - I$ relations). This requires derivation of a complex conductivity $\tilde{\sigma}(J)$ model; (2) explain experimental results which show that the macroscopic $V - I$ curve has no abrupt transition when J exceeds J_c; (3) obtain a temperature dependence of $n_s(T)$ which agrees with what is assumed in the two-fluid model; and (4) derive a general scheme for solving nonlinear electromagnetic problems in superconductors.

II. Distribution of Electrons

First it is assumed macroscopically that when an electron has an energy $E < E_c$, it is in superconducting state and paired with another electron; when $E \geq E_c$, it is in normal state. This characteristic energy E_c is a function of temperature T. For higher T, E_c is lower. At the critical temperature $T = T_c$, $E_c = 0$. Such characteristic E_c resembles the gap parameter Δ in the BCS microscopic theory. It may correspond to the de-pairing energy of a Cooper pair. But in this paper, this E_c is proposed as merely an assumption. The origin of this E_c should be studied in microscopic theory. We will leave this problem and use E_c as a starting assumption.

We assume the temperature dependence of E_c as

$$E_c(T) = 3.52 k_B T_c \left(1 - \frac{T}{T_c}\right)^{\alpha}, \quad \text{for } 0 \leq T \leq T_c \tag{1}$$

where k_B is the Boltzmann constant, T_c is the critical temperature, and α is a free parameter which may depend on the type of material ($\alpha > 0$ is required).

In macroscopic theory, the energy for each electron consists of kinetic energy and potential energy, $E = E_k + E_p = \frac{1}{2}mv^2 + E_p$, where m is the mass of an electron and v is its velocity. In quantum theory, v is the expectation value $<\psi|\hat{v}|\psi>$, where ψ is the wavefunction of the electron and $\hat{v}$ is the velocity operator. The electron energy E can be expressed as a function of temperature T, applied current density J, magnetic field H, and field frequency f, $E = E(T, J, f, H)$. E_c is the origin for critical values of T_c, J_c, f_c and H_c.

Consider a case where the electrons have one-dimensional velocities, for example, in a thin (radius $a \ll \lambda$ the penetration depth) wire within which the current flows in only one direction. The electrons in the sample have different velocities due to thermal motion. The average velocity of all electrons is nonzero along the current direction. The current density J is a macroscopic quantity. At a certain point $\vec{r}$, J is related to the average velocity of the electrons in a small volume ΔV,

$$J = \frac{\sum_i^N q v_i}{\Delta V} \tag{2}$$

where N is the number of electrons in ΔV and q is the charge of an electron. Note that not every electron has the same velocity. The velocities v_i of the electrons obey a certain distribution. Here we assume that the number of electrons, δN, which have the velocities between v and δv obeys a one-dimensional distribution. If we define

$$n(v) = \frac{\delta N}{\delta v \Delta V}, \tag{3}$$

then [10,11]

$$n(v) = n(v, v_A, n_0, m, k_B T) \tag{4}$$

where v_A is the average velocity of the electrons, m is the mass of an electron, and n_0 is the total number density of electrons in ΔV. Figure 1 shows a possible $n(v)$ function where $n(v)$ is assumed to be a continuous distribution of a Gaussian form. The specific mathematical form of the distribution $n(v)$ may be obtained from the microscopic quantum theory. If the wavefunction of each electron ψ_i is taken into account for a distribution $n(v_i)$, where $v_i = < \psi_i | \hat{v} | \psi_i >$, such formula can be derived from statistical physics. The numerical results shown in this paper are obtained by using the distribution in Figure 1.

We can relate the two macroscopic quantities, J and v_A by

$$J = \int_{-\infty}^{+\infty} qn(v) v dv = qn_0 v_A \tag{5}$$

at ΔV.

The T dependence of $n(v)$ requires that at $T = 0$,

$$n(v) = n_0 \delta(v), \tag{6}$$

a delta function [12]. For higher T, the spread of the distribution is wider.

III. $n_s(J)$ and Critical Current Density $J_c(T)$

Since the electrons have different velocities, and therefore different energies at a certain applied current density J, the electrons will not all exceed the E_c at the same time. The number density of superelectrons, n_s, does not disappear abruptly when J exceeds the macroscopic critical current density J_c. Only when $T = 0$ and $n(v)$ becomes $n_0 \delta(v)$, $n_s(J)$ shows an abrupt drop to zero at a critical $J_c(T = 0)$: for $J < J_c(0)$, $n_s = n_0$; and for

$J > J_c(0)$, $n_s = 0$. In experiments, since absolute $T = 0$K is not achievable, a completely sharp transition of n_s is not observed.

The $J_c(T)$ is related to the average velocity v_A and characteristic energy E_c. First, we define a characteristic velocity v_c for a single electron corresponding to E_c. If the potential energy is included in the case of maximum kinetic energy, $\frac{1}{2}mv_c^2 = E_c$. Hence, $v_c = \sqrt{2E_c/m}$. Since $J = n_0 q v_A$, we define

$$J_c(T) = qn_0 v_c = qn_0\sqrt{\frac{7.04k_BT_c}{m}}\left(1 - \frac{T}{T_c}\right)^{\alpha/2} \tag{7}$$

as the critical current density. This J_c is different from the Ginzburg-Landau's de-pairing current density. Here $J_c(T)$ is a quantity derived from the hypothetical characteristic energy E_c via the classical kinetic energy expression. For $T \neq 0$, $n_s(J)$ is a smoothly varying function and the sample is partially superconducting. The $J_c(T)$ has a different characteristics from J_c at $T = 0$. This smooth varying feature of the $I - V$ curve has been widely observed in experiments [5.6].

Since $v_A = J/qn_0$, the number density of superelectrons (here we count the single electron density rather than the pair density) $n_s(J)$ can be derived from the velocity distribution. The superelectrons are those whose energy are lower than E_c. In the one-dimensional case,

$$n_s(J) = \int_{-v_c(T)}^{v_c(T)} n(v)dv \tag{8}$$

In general, this integral can only be evaluated numerically.

At $T = T_c$, $v_c = 0$, hence $n_s = 0$ for all J's. By using the electron velocity distribution in Figure 1, $n_s(J)$ is plotted in Figure 2 for four different temperatures. Here J is normalized by the J_c at $T = 0$. At $T = 0$, $n_s = n_0$ for $J < J_c(0)$. This is what has been predicted by the two-fluid model.

The temperature dependence of n_s assumed in the two-fluid model is that

$$n_s(T) = n_0 \left[1 - (\frac{T}{T_c})^4\right].$$

The $n_s(T)$ function is compared with our distribution model in Figure 3. For a fixed J, the $n_s(T)$ curve matches the two-fluid model for $\alpha = 3/2$.

IV. Conductivities $\sigma_s(J)$ and $\sigma_n(J)$

To derive the constitutive relations of superconductors for electromagnetic fields, we will use the London's equations. The London's equations are derived from the fundamental Newtonian dynamics and the Meissner effect. They can also be derived from quantum mechanics by introducing a canonical momentum [3,8]. If we do not consider the Lorentz force due to magnetic field, the linear London's equations are valid from the Drude model and the Newton's second law.

$$\frac{\partial \overline{J}_s}{\partial t} = \frac{\overline{E}}{\Lambda} \tag{9}$$

$$\nabla \times \overline{J}_s = -\frac{\overline{B}}{\Lambda} \tag{10}$$

where $\overline{E}$ and $\overline{B}$ are the total electric and magnetic fields, respectively, $\overline{J}_s$ is the current density due to superelectrons, and $\Lambda = m_s/q_s^2 n_s$. The subscript s denotes that the quantity is of superelectrons. The nonlinearity will be included in $\Lambda(J) = \mu_0 \lambda^2$, and

$$\lambda(J) = \sqrt{\frac{m_s}{q_s^2 n_s(J) \mu_0}}. \tag{11}$$

Once $n_s(J)$ is known, $\lambda(J)$ can be derived. Hence, the nonlinear constitutive relations are obtained. Nonlinear effects come in Λ and n_s.

Substituting eq. (8) of $n_s(J)$ in λ, we derive the $\lambda(J)$ function, which is plotted in Figure 4. The penetration depth goes to infinity when $J \gg J_c(T)$. Conductivities $\sigma_s(J)$ and

$\sigma_n(J)$ are derived from the London equations for time-harmonic ($e^{-i\omega t}$) fields

$$\sigma_s = \frac{iq_s^2 n_s}{\omega m_s} \tag{12}$$

and

$$\sigma_n = \frac{q^2 n_n \tau}{m(1 - i\omega\tau)} \tag{13}$$

where

$$n_s(J) = \int_{-v_c(T)}^{v_c(T)} n(v)dv$$

and the number density of normal electrons $n_n(J) = n_0 - n_s(J)$ from conservation of charge. The above equations are the main results of this paper. The conductivities are plotted in Figures 5a and 5b, where τ is the transport time or the mean scattering time of normal electrons. $\sigma_s(J)$ and $\sigma_n(J)$ reflect the current dependence of n_s and n_n, respectively. These plots are for $T = 88$ K very close to the critical temperature $T_c = 90$ K. The nonlinear behavior is easy to see. Total conductivity is a complex number

$$\tilde{\sigma}(J) = \sigma_n(J) + \sigma_s(J) \tag{14}$$

V. Geometry Effect in Nonlinear Relations

1. Thin wire

For a thin wire superconductor with radius $a \ll \lambda$, the current density J can be assumed independent of the radius ρ. The thin wire is an ideal case since $a \ll \lambda$ is not practical. Usually $\tau \approx 10^{-12}$ sec, and $\omega < 10^9$ Hz, hence $\omega\tau \ll 1$ which is the quasi-static case. $\sigma_n \approx \frac{q^2 n_n \tau}{m}$. Here we can not assume $|\sigma_s| \gg |\sigma_n|$ since we are studying the transition region where n_s may become very small.

Resistance per unit length of the wire can be written as

$$R = \frac{|\sigma_n|}{[|\sigma_n|^2 + |\sigma_s|^2]\pi a^2}. \tag{15}$$

The kinetic inductance L_k per unit length of the wire can be written as

$$L_k = \frac{|\sigma_s|}{[|\sigma_n|^2 + |\sigma_s|^2]\omega\pi a^2}. \tag{16}$$

In this case, the internal and external inductances, L_{in} and L_{ex}, which are related to the energy stored in the magnetic field, are independent of I and therefore are linear. Figure 6 shows the calculated $R - I$ and $L_k - I$ curves from eqs. (15) and (16), where $\omega\tau = 10^{-3}$, $I = J\pi a^2$. The $R - J$ curve appears very nonlinear because $T = 88$ K is very close to $T_c = 90$ K. One interesting behavior in the $L_k - J$ curve is that the maximum L_s appears near J_c. This can be explained from eq. (16). At $J \ll J_c(T)$, $n_s \gg n_n\omega\tau$, hence $L_k \approx 1/n_s$ is small. At $J \gg J_c(T)$, $n_n\omega\tau \gg n_s$, hence, $L_k \approx n_s/(n_n)^2$ is also small. When $n_n\omega\tau$ and n_s are comparable, a maximum of L_k may be achieved.

A special case is at DC when $\omega = 0$. From eq. (12), $\sigma_s \to \infty$. From the first London equation, $\overline{E} = \frac{\partial \overline{J}_s \Lambda}{\partial t} = 0$. When $J \gg J_c$, $n_s \to 0$, then it is possible for $\overline{E} \neq 0$. If J_s has a small time fluctuation, then $\frac{\partial}{\partial t}$ is not exactly zero and the above quasi-static discussion can be applied.

2. Slab and thin film strip

The above discussion has not taken into account the geometry of the superconductor. For superconductors with finite dimensions, e.g., a slab in Figure 7, the non-uniform distribution of current density $J_y(x)$ will cause the nonlinearity to occur earlier in the $R - I$ and $L_k - I$ curves. The internal and external inductances L_{in} and L_{ex} will also be nonlinear since $J_y(x)$ is determined by I,

$$I = \iint J_y ds = \int dz \int dx J_y(x) = \int dz \int dx \tilde{\sigma}(x) E(x) \tag{17}$$

where $E(x)$ is the electric field. For a uniform current density, $J_y(x) = J_A$, $J_A = I/\Delta z d$ where d is the thickness of the slab. For non-uniform $J_y(x)$, J_y is bigger than J_A at the edge of the slab and $n_s(J)$ is smaller at the edge. Therefore, for the same magnitude of I, inhomogeneous $J_y(x)$ will exceed J_c at some x's even when J_A is less than J_c.

If a three-dimensional velocity distribution is considered for a current flow in the y direction, $J_y = qn_0v_A$ and

$$\lim_{T\to 0} n(\overline{v}) = n_0\delta(v_x)\delta(v_y - v_A)\delta(v_z) \tag{18}$$

$$n_s(J_y) = \int_{-v_c}^{v_c} dv_y \int_{-\sqrt{v_c^2-v_y^2}}^{\sqrt{v_c^2-v_y^2}} dv_x \int_{-\sqrt{v_c^2-v_y^2-v_x^2}}^{\sqrt{v_c^2-v_y^2-v_x^2}} n(\overline{v})dv_z \tag{19}$$

with $v_A = J_y/qn_0$.

Under the quasi-static condition $\omega\tau \ll 1$, if a current I is applied along y direction in the slab, a magnetic field $H_z(x)$ will result from the applied current $J_y(x)$. Note that in the finite-width slab of a linear superconductor, even at $\omega = 0$, current $J_y(x)$ has a non-uniform distribution, due to the penetration depth λ. From the second London equation (10) and $\nabla \times \overline{A} = \overline{B}$, $\nabla \times \overline{H} = \overline{J}$, under the London gauge, $\nabla \cdot \overline{A} = 0$ and

$$\overline{A} = -\Lambda \overline{J}_s, \tag{20}$$

$$\nabla^2[J_s\lambda^2(J)] = J_s + J_n = J \tag{21}$$

where $\overline{A}$ is the vector potential. In general, this equation can not be solved in a closed-form.

We first consider the solution of a linear superconductor for $n_s \gg n_n\omega\tau$.

$$J_y(x) = \frac{I}{2\lambda}\frac{\cosh(x/\lambda)}{\sinh(d/2\lambda)} \quad \text{for } |x| \le d/2 \tag{22}$$

and

$$H_z(x) = -\frac{I}{2}\frac{\sinh(x/\lambda)}{\sinh(d/2\lambda)} \quad \text{for } |x| \le d/2. \tag{23}$$

An iterative scheme for solving the nonlinear problem is to initially use the linear solution $J_y(x)$ in eq. (22) to calculate $n_s(J)$ in eq. (8) and $\lambda(x)$ in eq. (11). Then λ in eq. (22) is substituted with the $\lambda(x)$ obtained to calculate $J_y(x)$. Then eq. (8) is used to calculate $n_s[J_y(x)]$ again. This procedure is repeated until $J_y(x)$ converges. Figure 8 shows the results of $J(x)$ and $\sigma_s(x)$ obtained from the iterative method.

The impedance of the slab is defined as

$$Z = \frac{1}{\int_{-d/2}^{d/2} dx \tilde{\sigma}(x)} \tag{24}$$

and resistance $R = Re(Z)$ and kinetic inductance $L_k = -Im(Z)/\omega$. Figure 9 shows the $R - I$ and $L_k - I$ relations from the final convergent $J_y(x)$.

For different thickness d, the nonlinear curve will be different. We have found that for smaller d/λ, $R - I$ and $L_k - I$ relations are more nonlinear. This is understandable since J_y is bigger for smaller d for a given applied current I.

Surface impedance of a superconductor is defined as

$$Z_s = \sqrt{\frac{\mu_0}{\tilde{\epsilon}}} \tag{25}$$

where

$$\tilde{\epsilon} = \epsilon + \frac{i\tilde{\sigma}(J)}{\omega}. \tag{26}$$

Surface resistance is $R_s = Rc(Z_s)$, and surface inductance is $L_s = -Im(Z_s)/\omega$. For $\omega\tau = 10^{-3}$, R_s and L_s are plotted in Figure 10. The nonlinear region appears near J_c where the sample is partially superconducting. In the normal or superconducting states, the relations are linear. The L_s is different at normal and superconducting regions. Experimental results [13] are compared in Figure 11. As it shows, this model agrees with the trend of the experimental results. Since some parameters (α, τ, etc.) are material dependent,

by adjusting these parameters, a better fit between the theory and measurement may be found. Surface impedance Z_s is a good description of superconductors since most of the currents and fields are confined within the penetration depth λ from the surface.

Another case of interest is at very high frequencies and σ_n for $T > T_c$ is not very big (which is true for the ceramic high T_c superconductors) so that ϵ can not be neglected in eq. (26) for J_y near J_c. Since $\frac{\partial}{\partial t} \neq 0$ in the Maxwell's equations, a wave equation has to be considered. We will solve the guided wave case where the electric field E_y is decaying away outside the slab.

The wave equation for E is

$$\nabla^2 E + k_0^2 \tilde{\epsilon_r} E = 0 \tag{27}$$

where

$$\tilde{\epsilon_r} = 1 + \frac{i\sigma(\tilde{J})}{\omega \epsilon_0}. \tag{28}$$

If we replace E by $\tilde{\sigma} J_y$ in eq. (27), (27) will look very similar to (21). We can also use an iterative scheme to solve for the nonlinear $\tilde{\sigma}$ case. First, we assume σ is independent of J and solve for $J_y(x)$. Second, we calculate $\sigma(x) = \sigma[J_y(x)]$. Third, we solve the wave equation for the inhomogeneous medium problem and obtain $J_y(x)$. These steps will be repeated until $J_y(x)$ and $\tilde{\sigma}(x)$ converge. This is a feed-back process. At the edge, increase in J_y will cause n_s to decrease, which causes σ_s, and hence J_y to decrease. This will continue until the a stable solution is obtained.

This procedure is similar to solving coupled two differential equations in the GL theory where the equation for $\overline{A}$ is essentially the same as the wave equation (27) for E or J_y. The difference is the second equation for ψ, where $\psi(\overline{A})$ ($n_s(J)$) is to be derived. We have derived $n_s(J)$ in this paper from the velocity distribution assumption.

The results for the slab geometry can be used to study a microstrip geometry. If the dimension of z in Figure 7 is reduced to $d \ll \lambda$, the current will still be uniform in the z direction. Therefore, the same results can be applied.

This nonlinear model can also be applied to study the dependence of R and L on the magnetic field H. Once the relation between the magnetic field H and the current J is determined, H_c and J_c can be related and the above discussion is directly applicable.

Although the model presented is classical, the corresponding quantum statistical distribution can be used to derive the velocity (energy) distribution. Discrete distribution may be needed if the energy is quantized.

VI. Conclusion

A macroscopic model is proposed for nonlinear constitutive relations in superconductors. Distribution of electron velocities is used to derive the dependence of superelectron density n_s on applied macroscopic current density J. Complex $\tilde{\sigma}(J)$ is obtained. The geometry of a superconductor will introduce non-uniform distribution of the current density J. Therefore, nonlinearity will be enhanced at the edges and surfaces of superconductors. Using this macroscopic model, a solution scheme for electromagnetic properties of superconductors has been proposed.

Acknowledgment

This work was supported in part by the US Office of Naval Research under contracts N00014-89-J-1019 and N00014-90-J-1002.

References

[1] P. England, et al., "Granular superconductivity in $R_1Ba_2Cu_3O_{7-\delta}$ thin films", Phy. Rev. B, Vol.38, No.10, pp. 7125-7128, Oct. 1988.

[2] M.A. Dubson, et al., "Non-Ohmic regime in the superconducting transition of Polycrystalline $Y_1Ba_2Cu_3O_x$", Phy. Rev. Lett., vol. 60, no. 11, pp. 1061-1064, March 1988.

[3] T. Van Duzer and C.W. Turner,"Principles of Superconductive Devices and Circuits", New York: Elsevier, 1981.

[4] G.J. Chen and M.R. Beasley, "Shock-wave generation and pulse sharpening on a series array Josephson junction transmission line," IEEE Trans. on Appl. Supcond., vol. 1, no. 3, Sept. 1991.

[5] D.H. Kim, et al., "Possible origins of resistive tails and critical currents in high-temperature superconductors," Phys. Rev. B. , vol. 42, No. 10, pp. 6249-6258, 1990.

[6] X. Yu and M. Sayer, "Temperature dependence of critical currents in YBaCuO ceramics," Phys. Rev. B., vol. 44, No. 5, 1991-I.

[7] L. N. Shehata, "The wall energy and the critical current of an anisotropic high-temperature superconductor using modified Ginzburg-Landau Theory," J. Low Temperature Phys. , vol. 78, No. 1/2, 1990.

[8] M. Tinkham, "Introduction to Superconductivity," McGraw-Hill Book Inc. , 1975.

[9] K.K. Mei and G.C. Liang, "Electromagnetics of superconductors", IEEE Trans. MTT. vol. 39, No. 9, Sept. 1991.

[10] L.D. Landau and E.M. Lifshitz, "Statistical Physics", Addison-Wesley, 1969.

[11] G.H. Wannier, "Statistical Physics", John Wiley & Sons, 1966.

[12] C.M. Bender and S.A. Orszag, "Advanced Mathematical Methods for Scientists and Engineers," McGraw-Hill Book Com. , 1978.

[13] Y. Kobayashi, T. Imai and H. Kayano, "Microwave measurements of temperature and current dependences of surface impedance for high-T_c superconductors," IEEE Trans. on Microwave Theory and Techniques, vol. 39, No. 9, pp. 1530-1538, Sept. 1991.

Figure Captions

Fig. 1. An assumed distribution of electron velocities for $T = 20$ K.

Fig. 2. Superelectron number density $n_s(J)/n_0$ at different temperatures. In this example, $\alpha = 3/2$, and $T_c = 90$K. $J_c(0)$ is from eq. (7).

Fig. 3. Comparison between the two-fluid model and this model for $n_s(T)/n_0$ at $J = 0$. Here $\alpha = 3/2$ and $T_c = 90$ K.

Fig. 4. Penetration depth λ as a function of current density J at $T = 88$K. Here $T_c = 90$ K.

Fig. 5. At $T = 88$K, $T_c = 90$K, (a) super-conductivity σ_s as a function of J. (b) normal conductivity σ_n as a function of J.

Fig. 6. At $T = 88$K, $T_c = 90$K, (a) resistance of a thin wire R as a function of J. (b) kinetic inductance L_k of a thin wire as a function of J.

Fig. 7. A superconducting slab with a thickness d.

Fig. 8. At $T = 80$K, $T_c = 90$K, $d/\lambda(J = 0) = 2$, (a) current density $J_y(x)$ distribution in a slab. (b) super-conductivity $\sigma_s(x)$ distribution in a slab.

Fig. 9. For $d/\lambda(J = 0) = 0.5, 1, 2$, $T_c = 90$K, (a) resistance of a slab, R, as a function of applied current intensity I at $T = 80$K; (b) kinetic inductance L_k of a slab as a function of applied current intensity I at $T = 80$K. Here $T_c = 90$K.

Fig. 10. At $T = 88$K, $T_c = 90$K, (a) Surface resistance R_s as a function of J, (b) surface

inductance L_s as a function of J.

Fig. 11 R_s as a function of surface current density K at $T = 77$K. The circles are the measured data from reference [13]. The sample is a YBCO at $f = 10.4$GHz with $T_c = 92$K. The solid curve is from this model, where $\alpha = 3/2$, and $\omega\tau = 2.8 \times 10^{-2}$. The surface current density is calculated from J with a thickness of $\lambda(J)$.

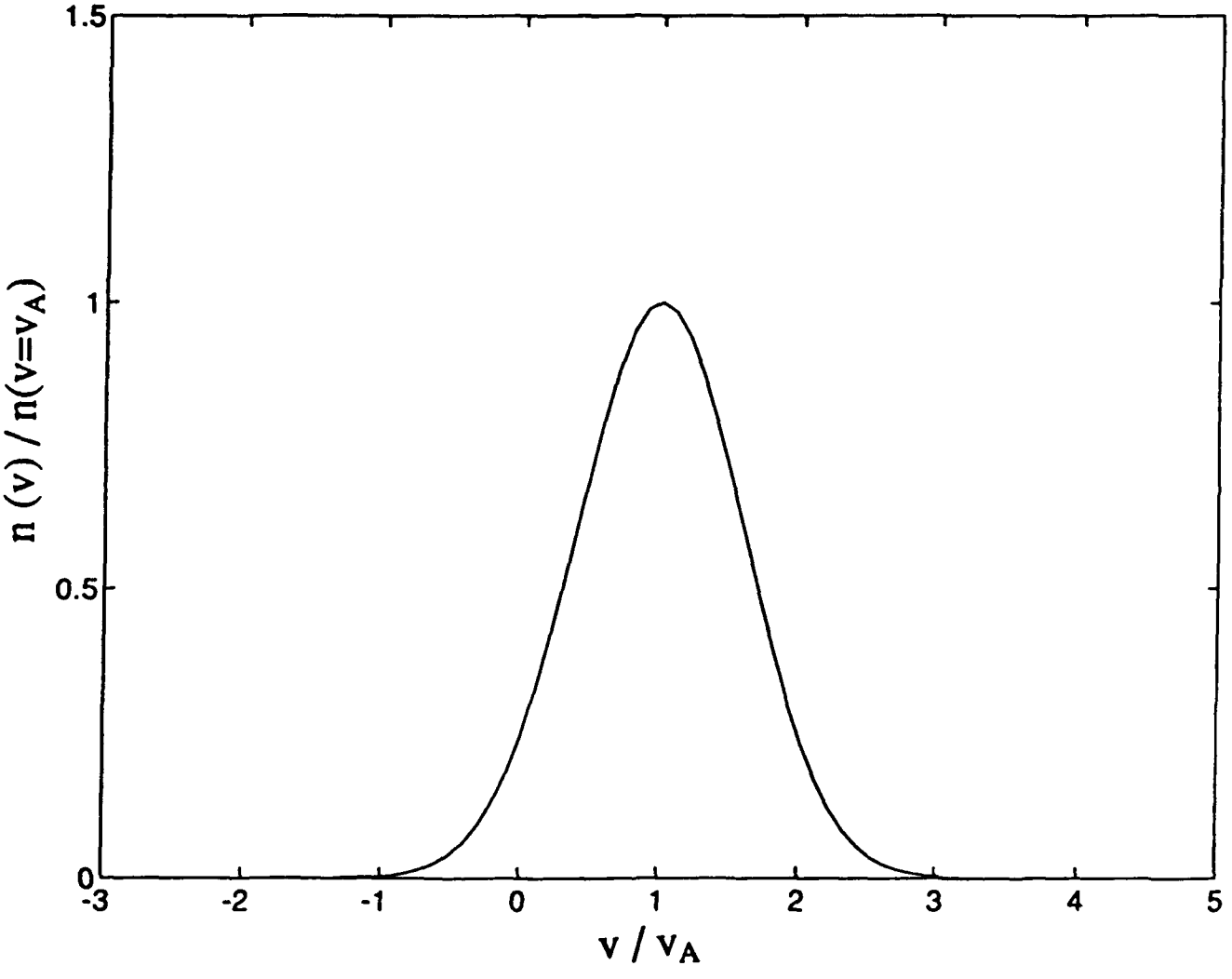
1.5
1
0.5
0
-3
-2
-1
0
1
2
3
4
5
n (v) / n(v=v_A)
v / v_A

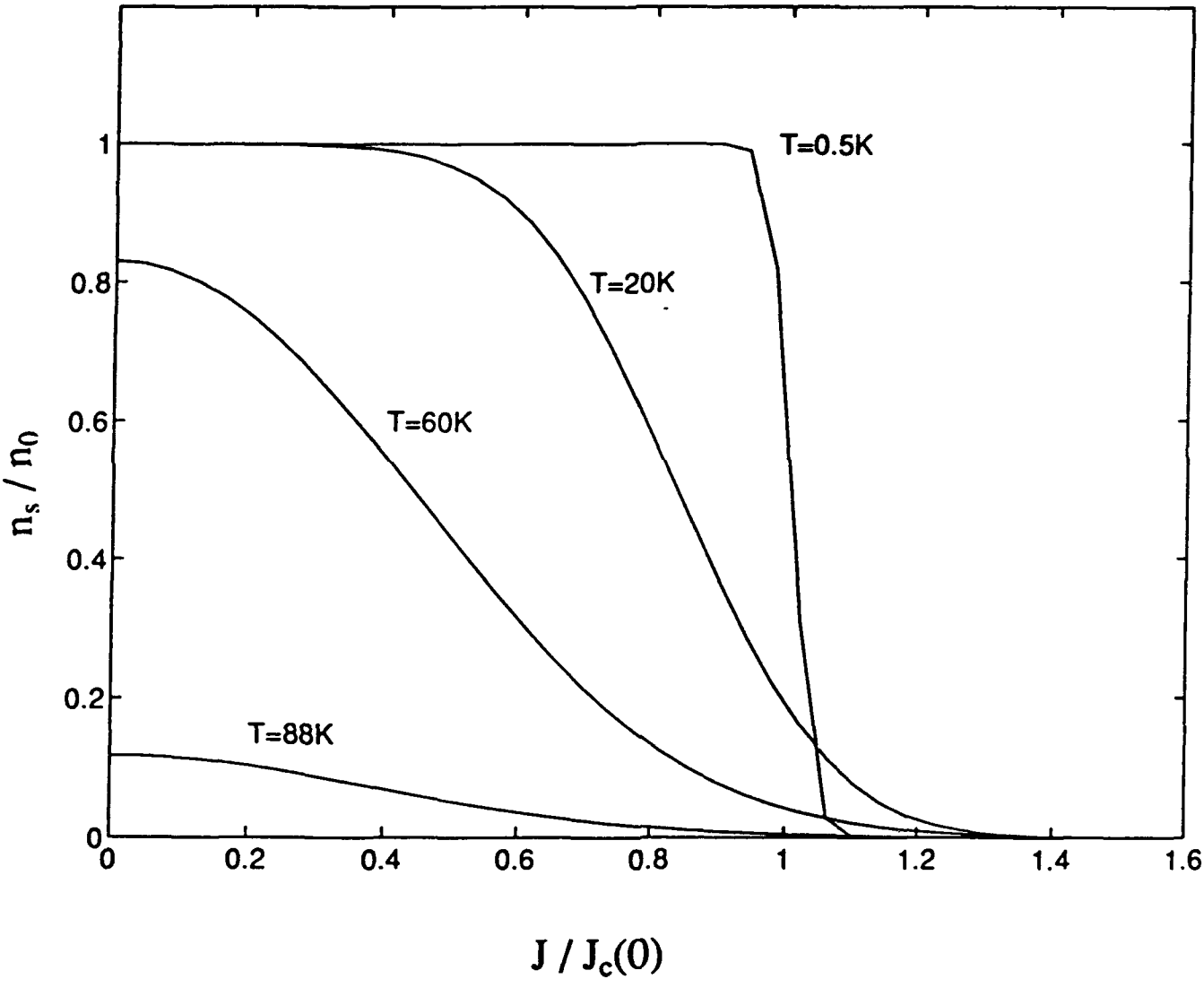
T=0.5K
T=20K
T=60K
T=88K
1
0.8
0.6
0.4
0.2
0
0
0.2
0.4
0.6
0.8
1
1.2
1.4
1.6
n_s / n_0
$J / J_c(0)$

Fig. 2

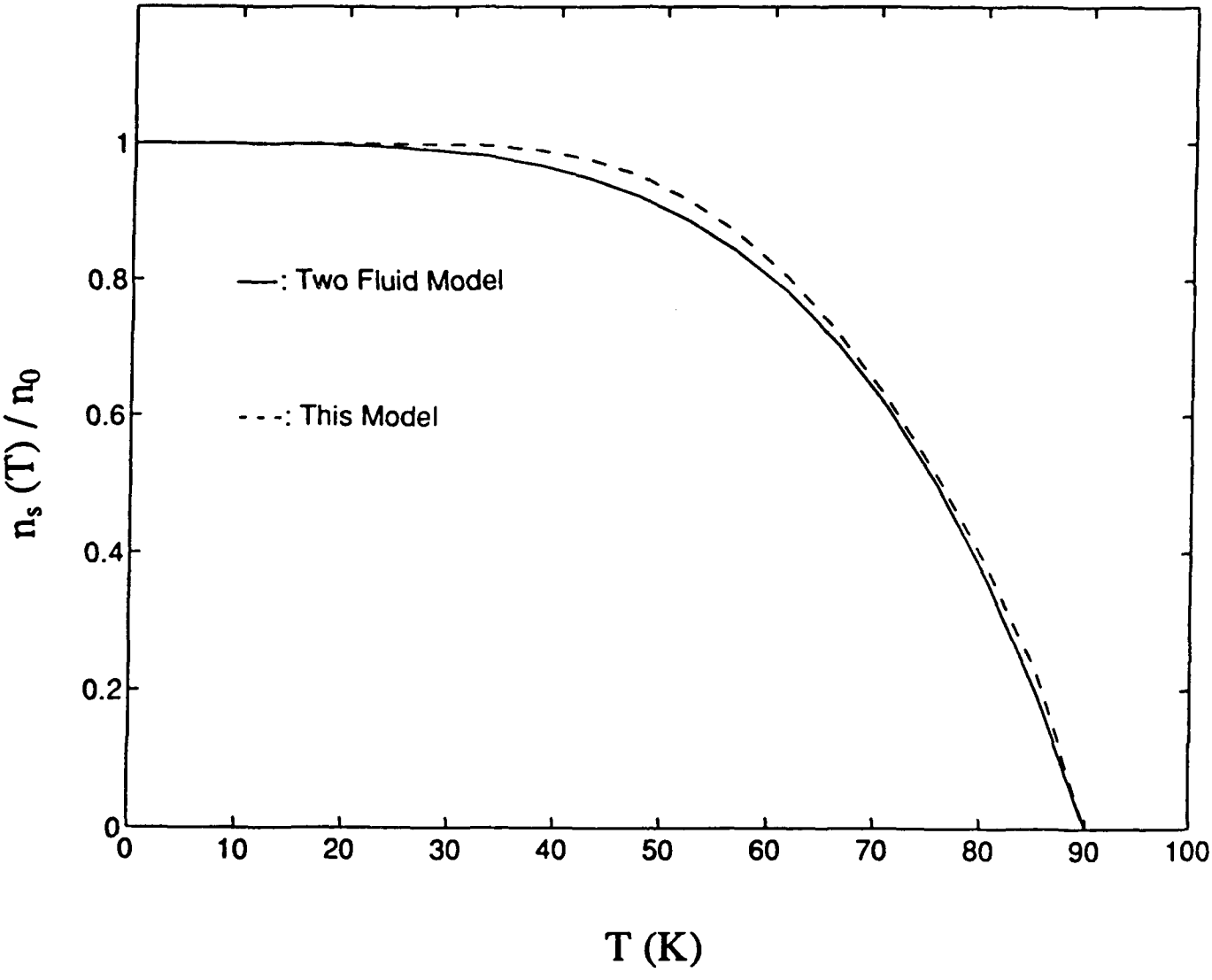
1
0.8
0.6
0.4
0.2
0
0
10
20
30
40
50
60
70
80
90
100
—: Two Fluid Model
- - -: This Model
n_s (T) / n_0
T (K)

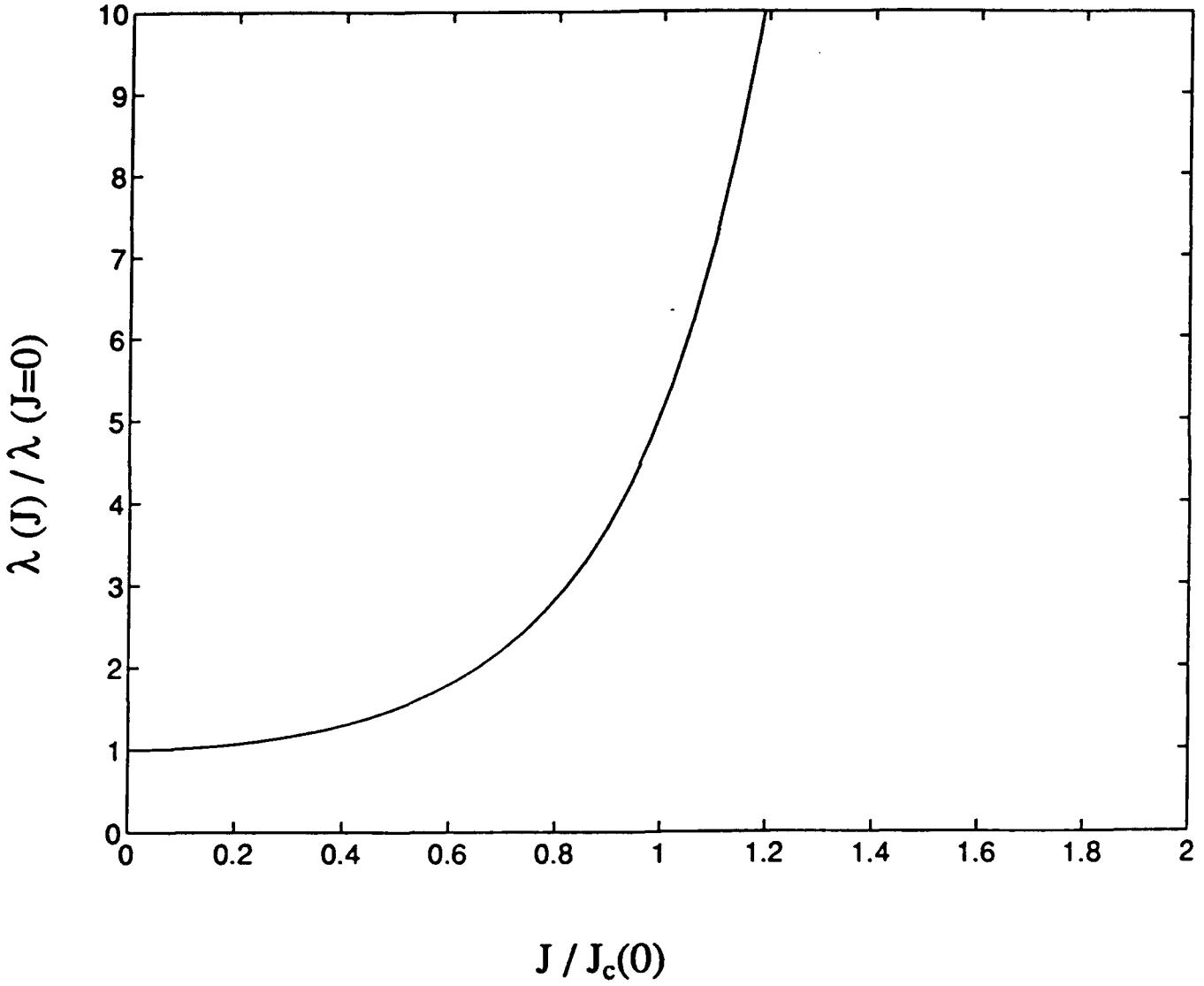

Fig. 4

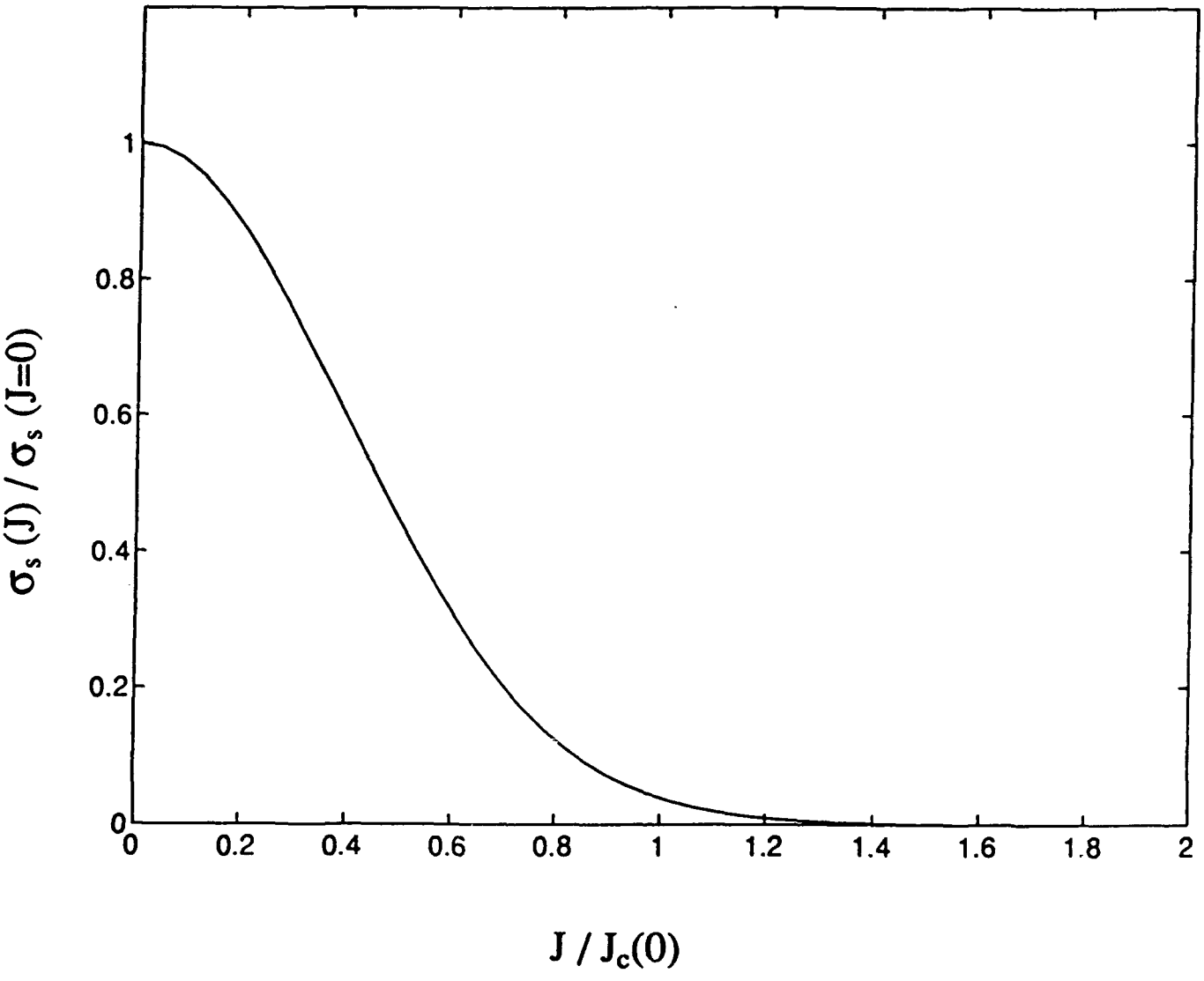

Fig. 5a

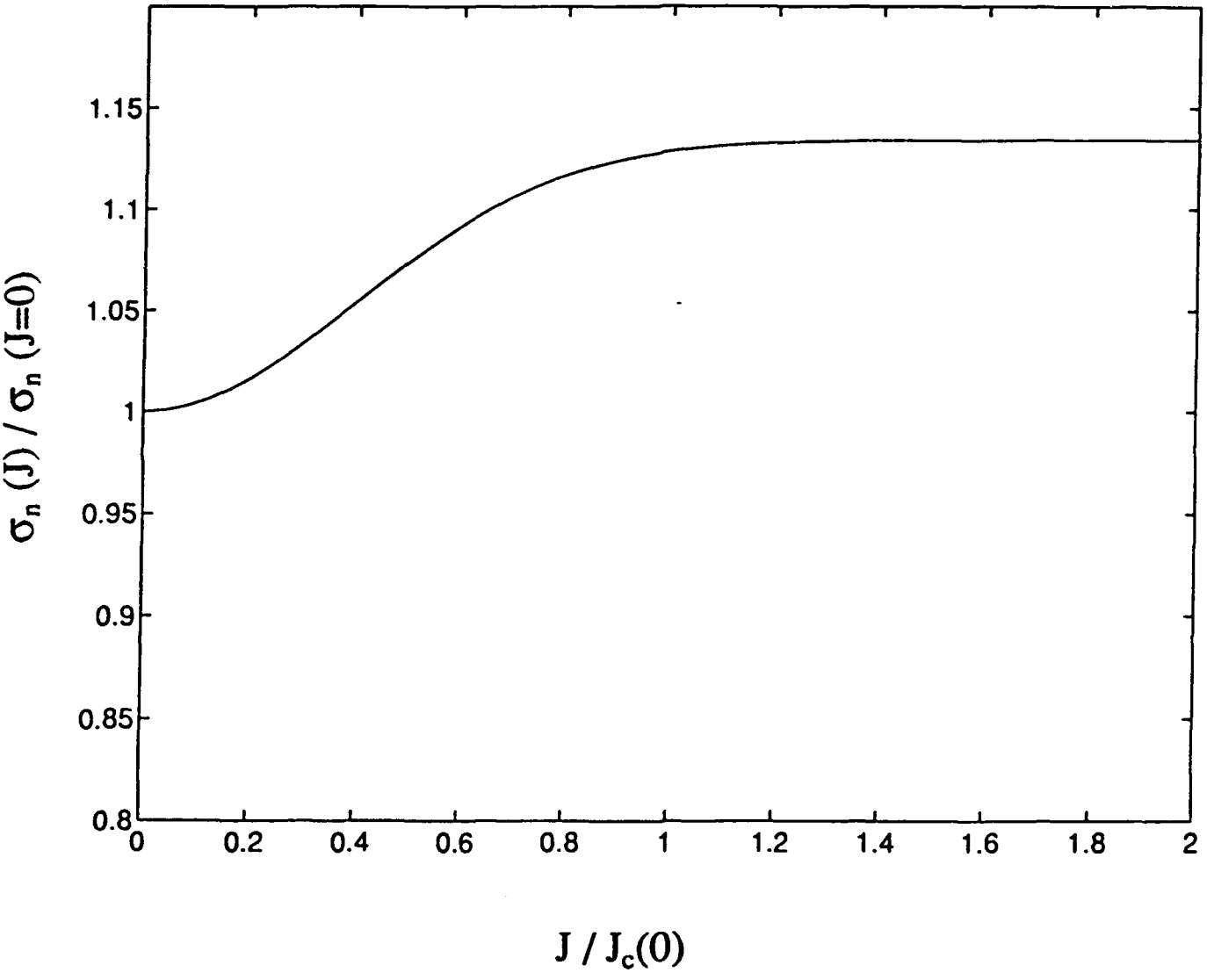

Fig. 5b

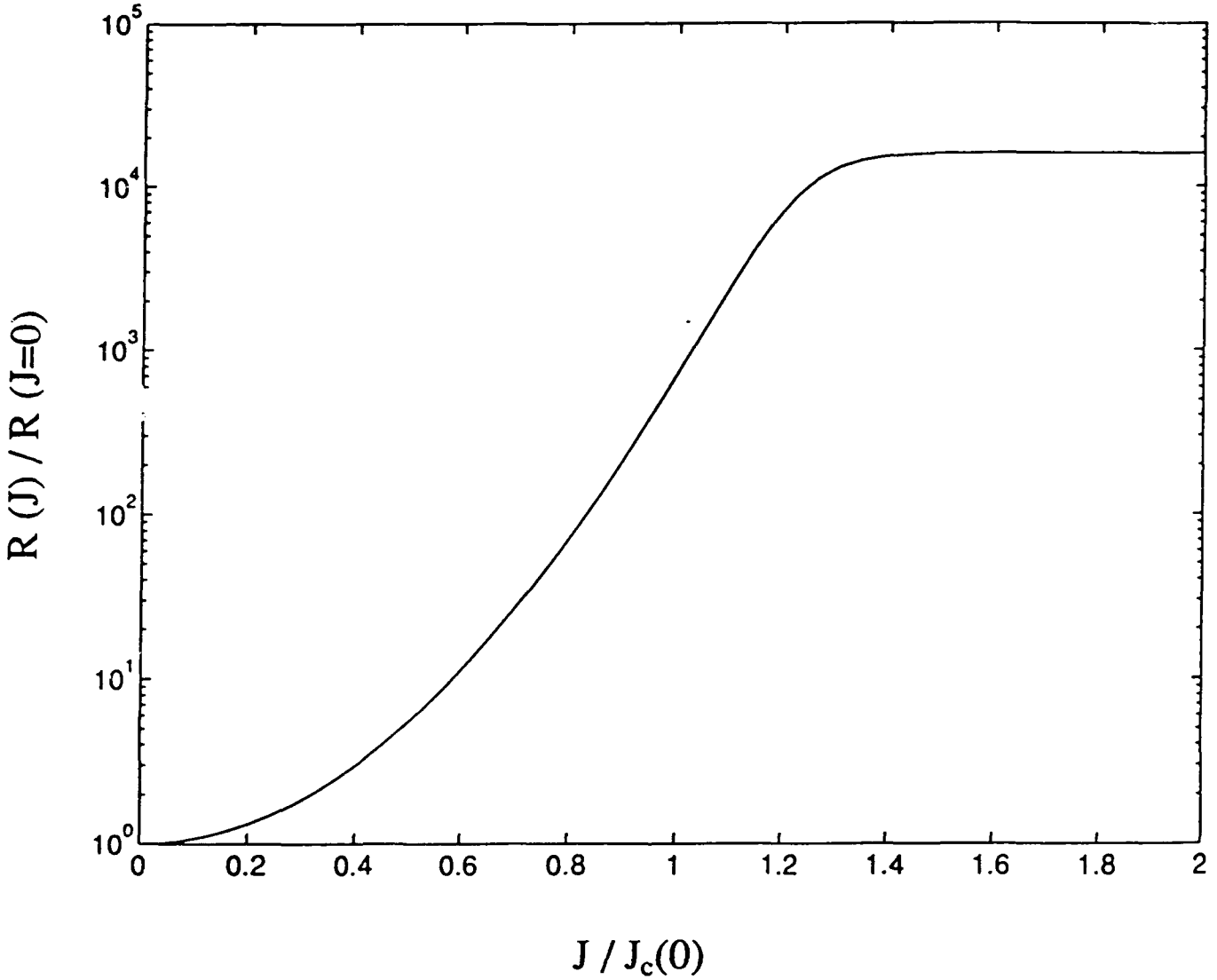

Fig. 6a

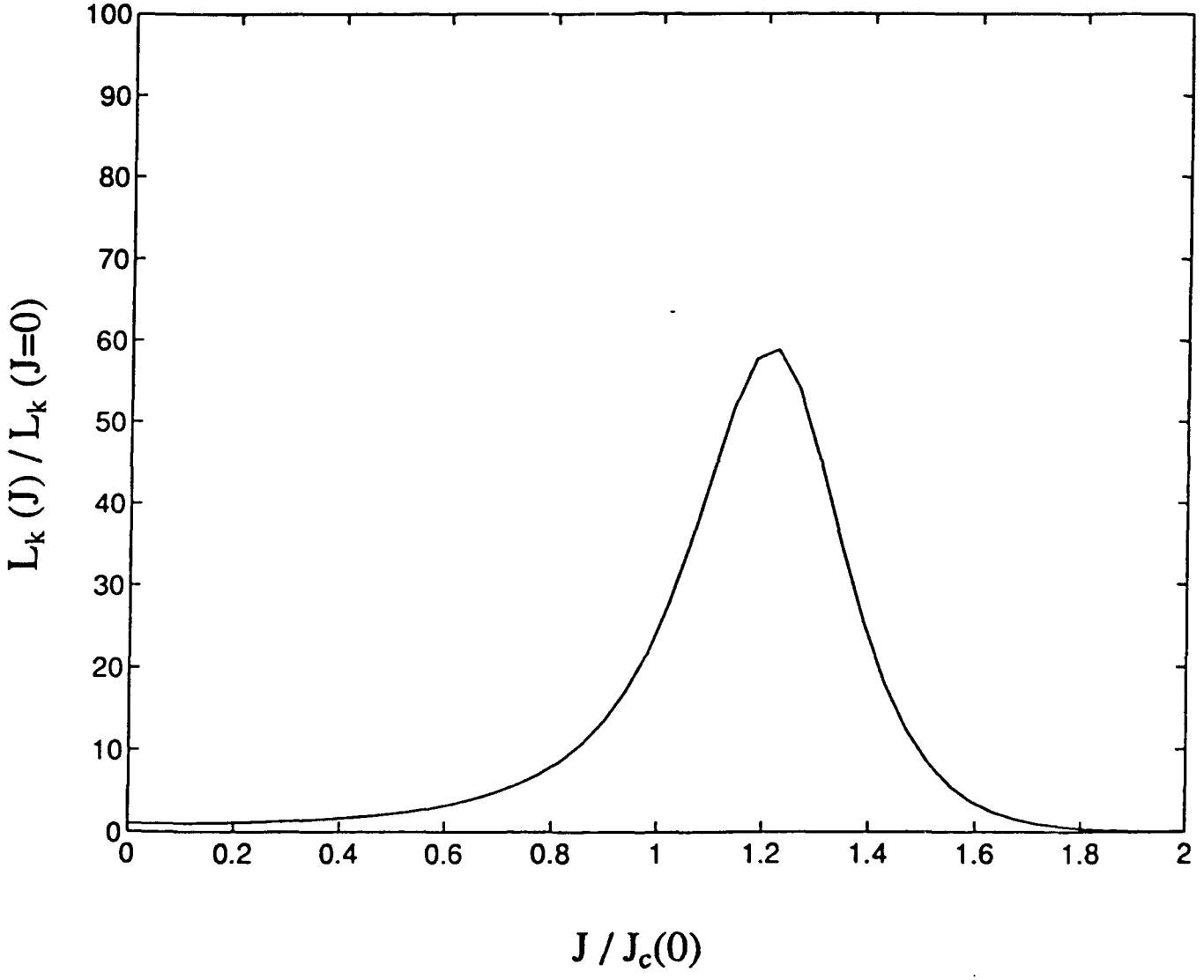
100
90
80
70
60
50
40
30
20
10
0
0
0.2
0.4
0.6
0.8
1
1.2
1.4
1.6
1.8
2
L_k (J) / L_k (J=0)
J / J_c(0)

Fig. 6b

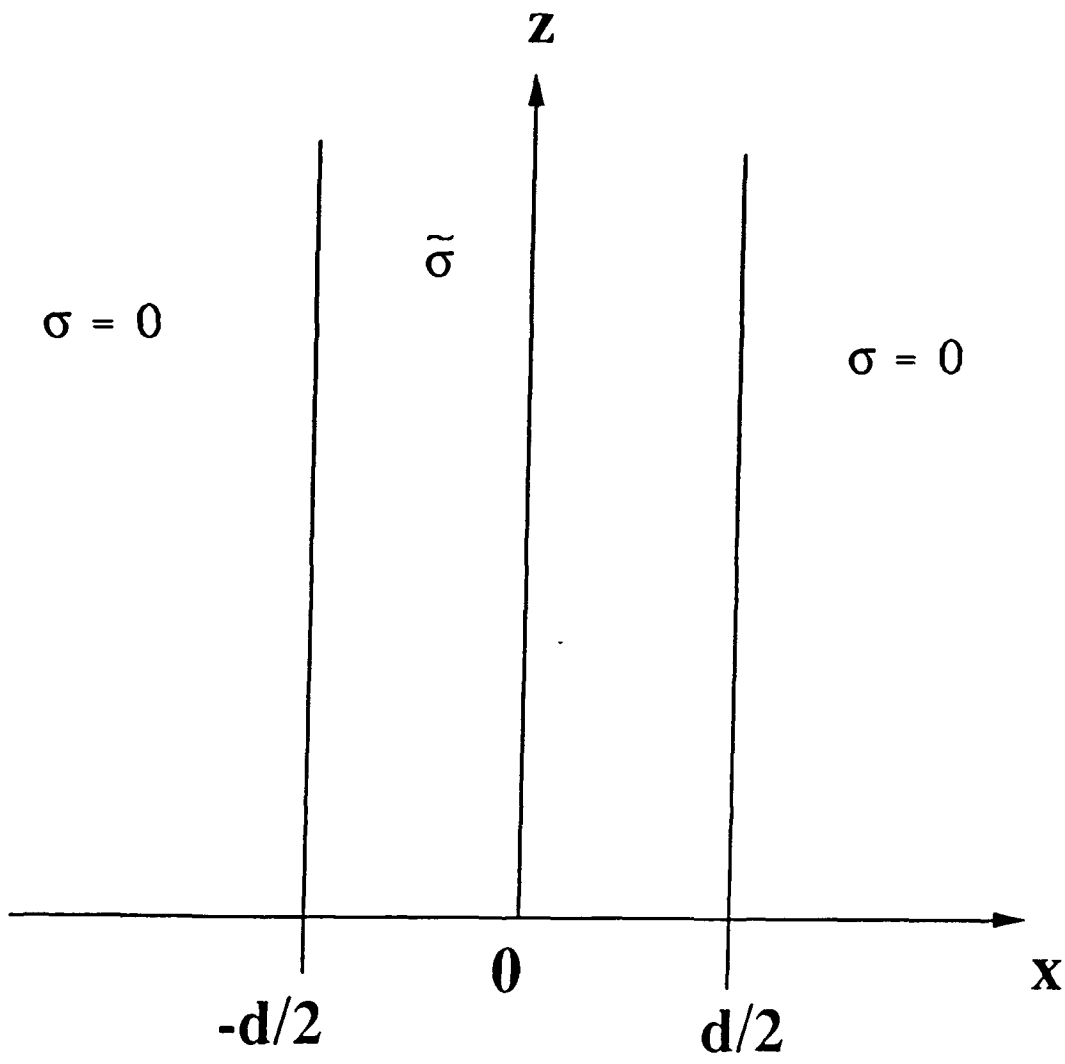
z
σ̃
σ = 0
σ = 0
0
x
-d/2
d/2

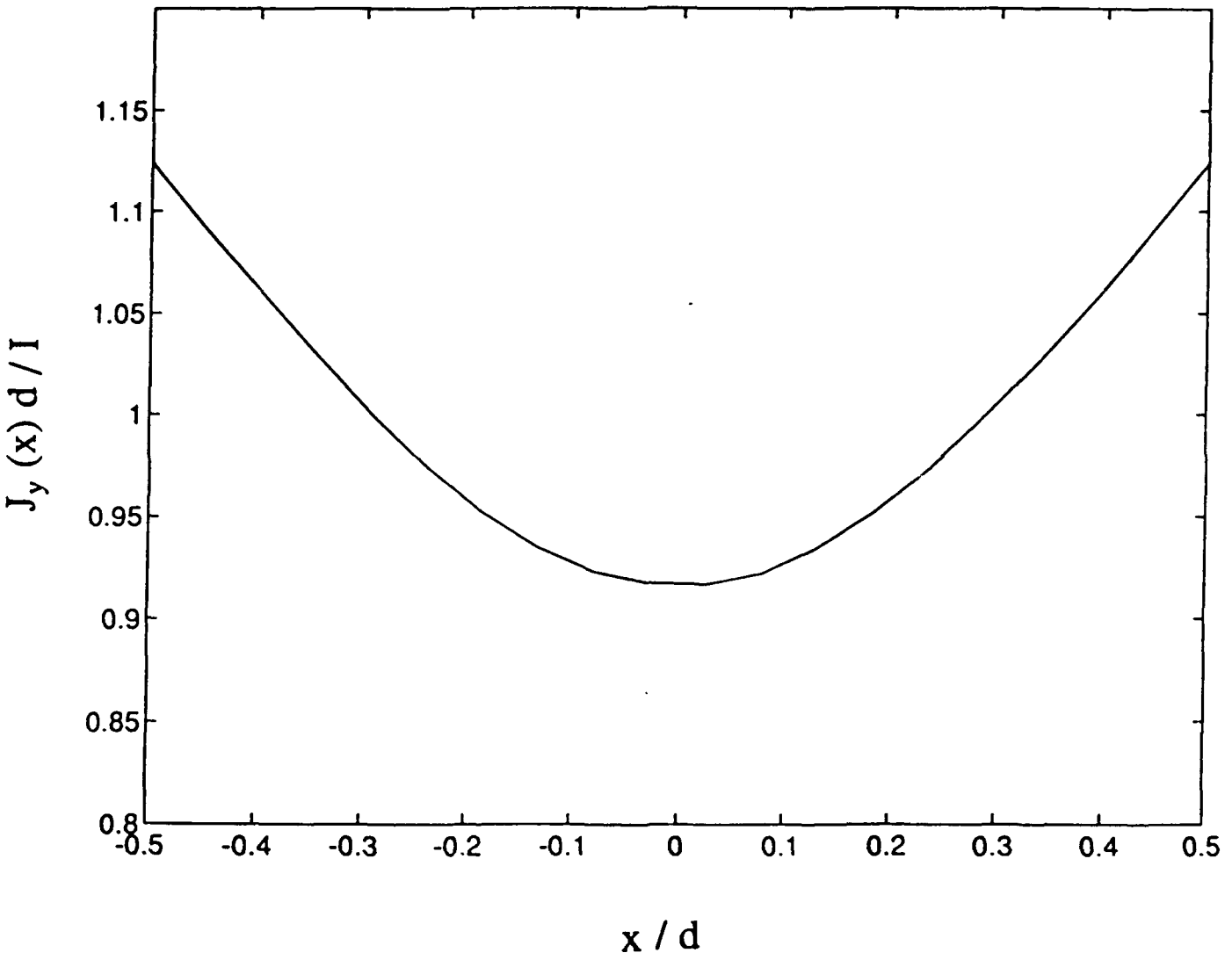

Fig 8a

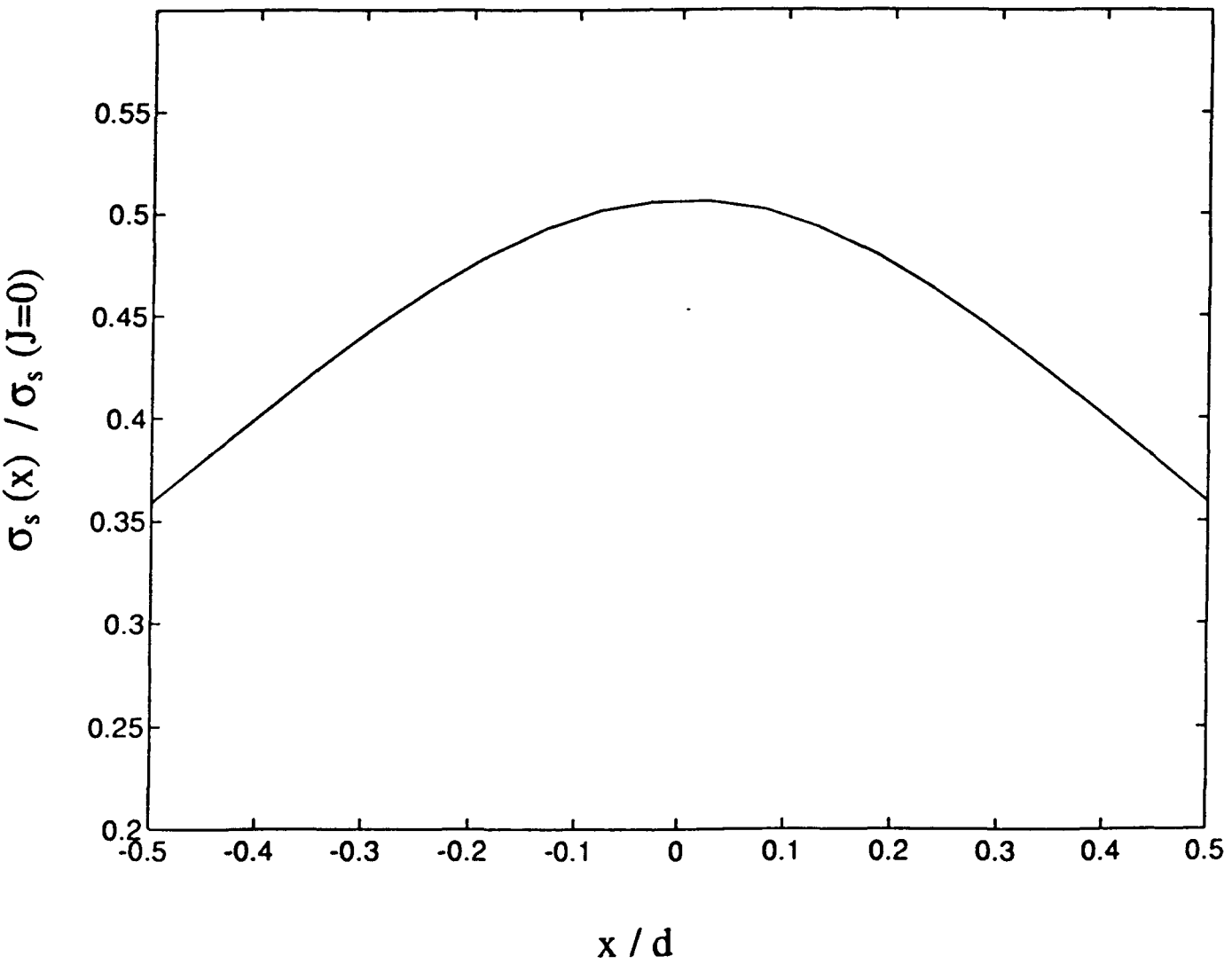
0.55
0.5
0.45
0.4
0.35
0.3
0.25
0.2
-0.5
-0.4
-0.3
-0.2
-0.1
0
0.1
0.2
0.3
0.4
0.5
σs (x) / σs (J=0)
x / d

Fig. 8b

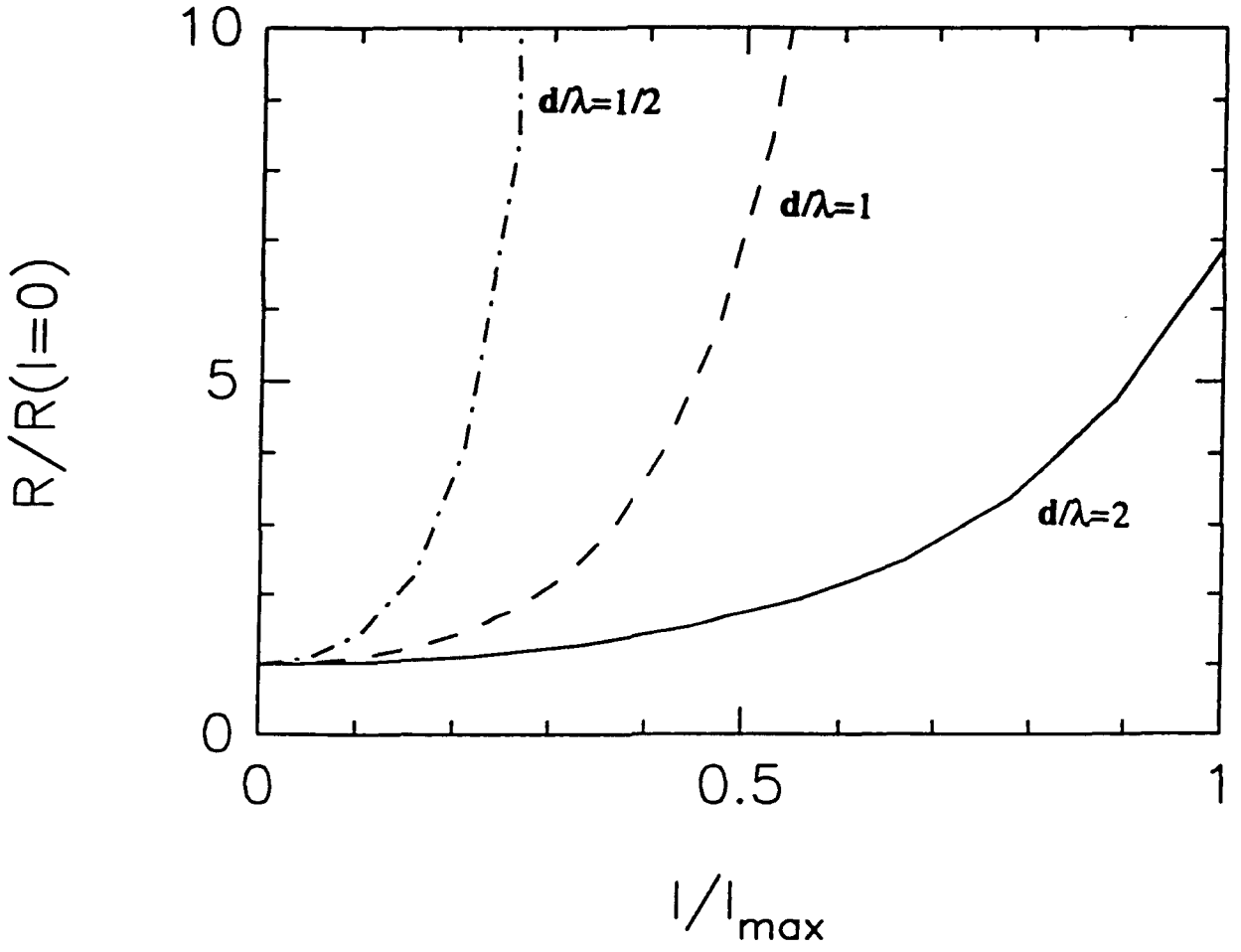

Fig 9a

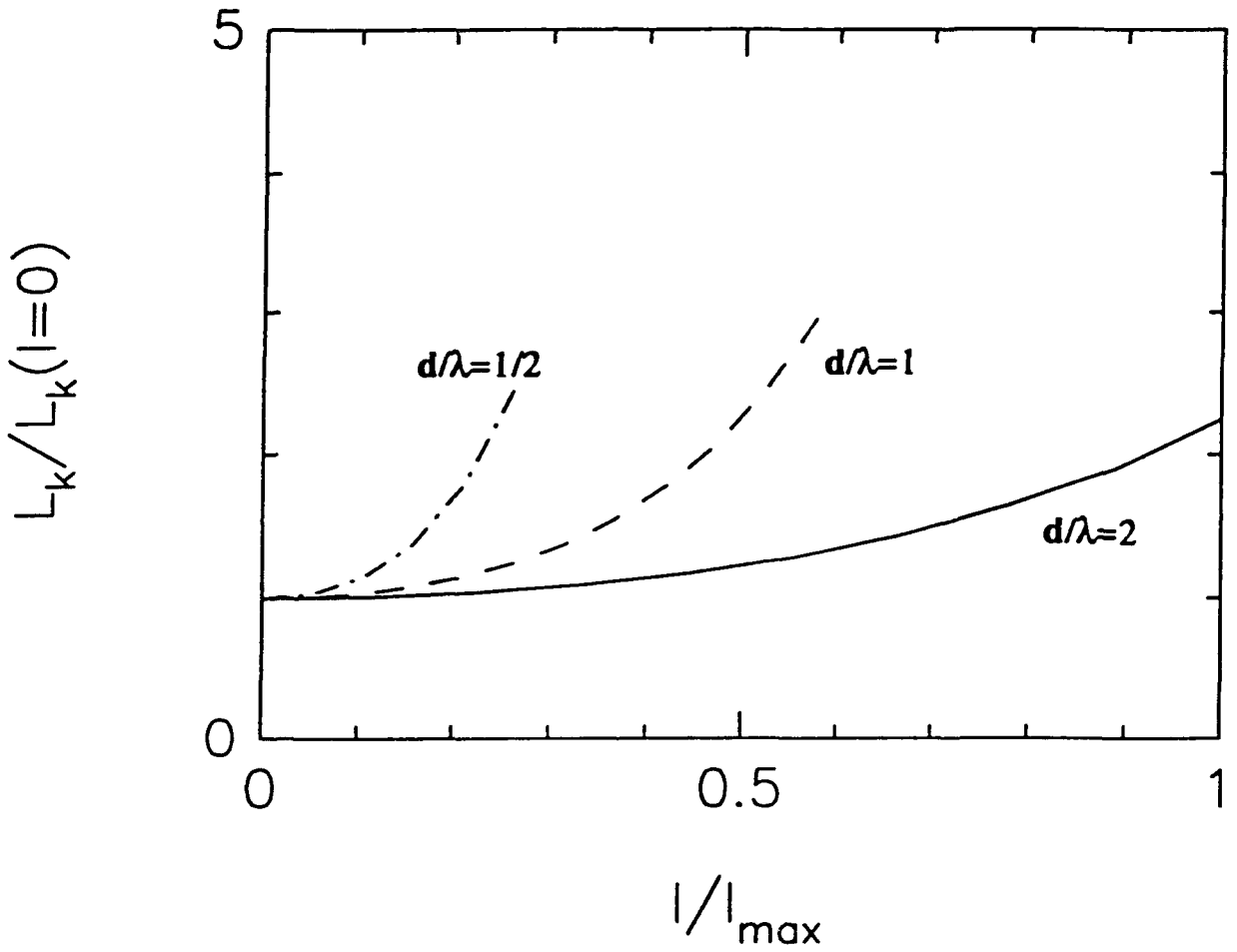

Fig 9b

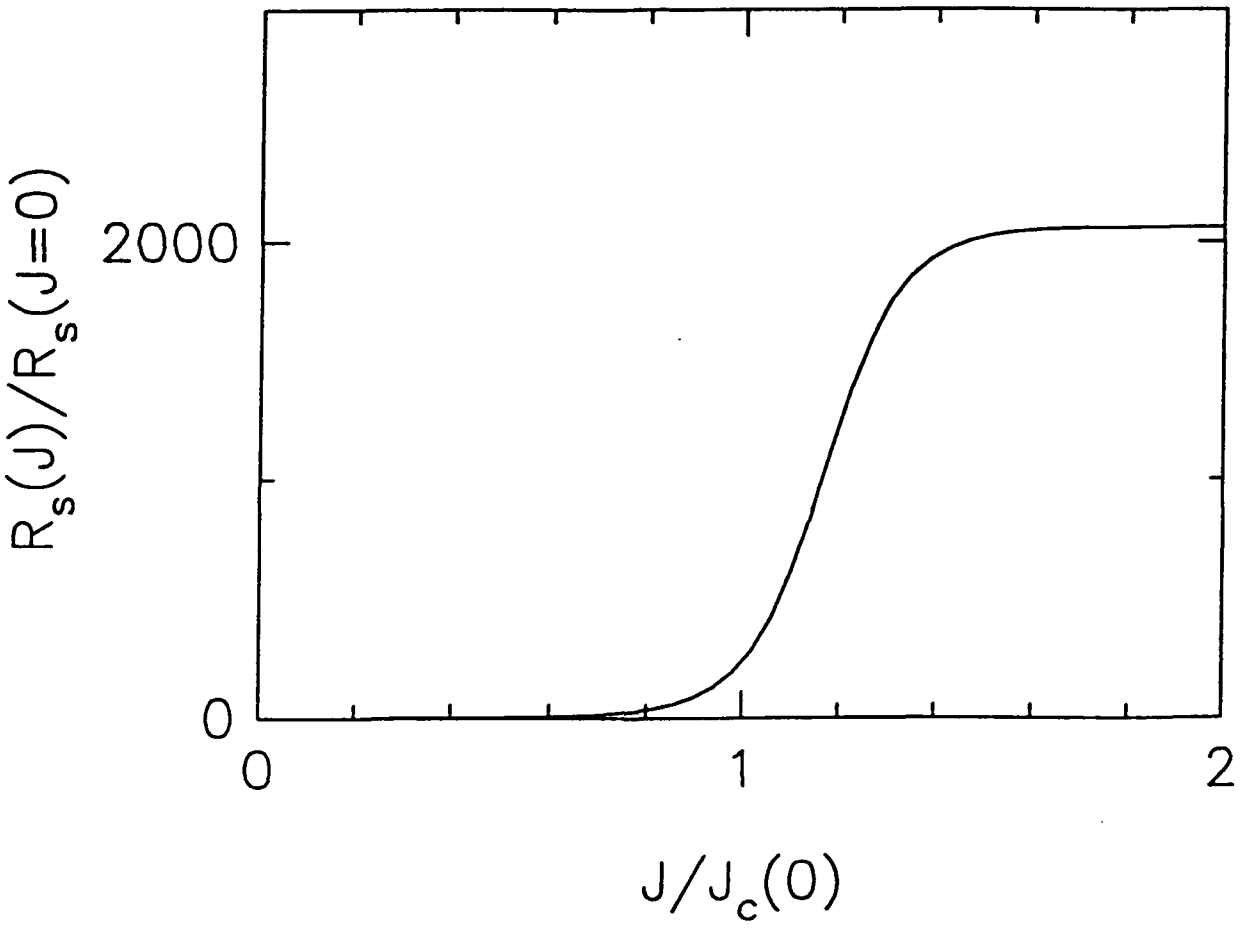

Fig. 10a

XIA 3-MAR-1992 20:44

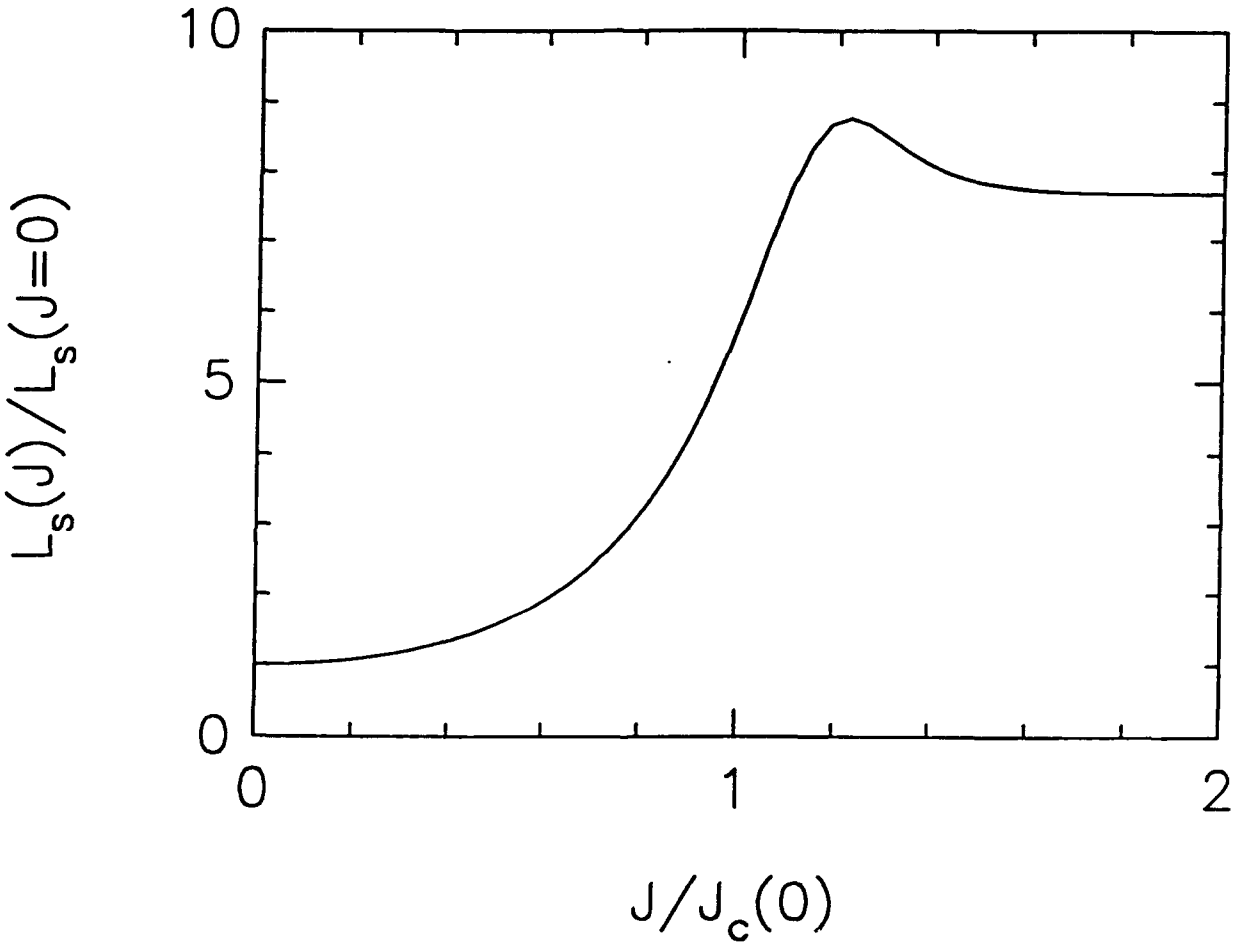

Fig 10b

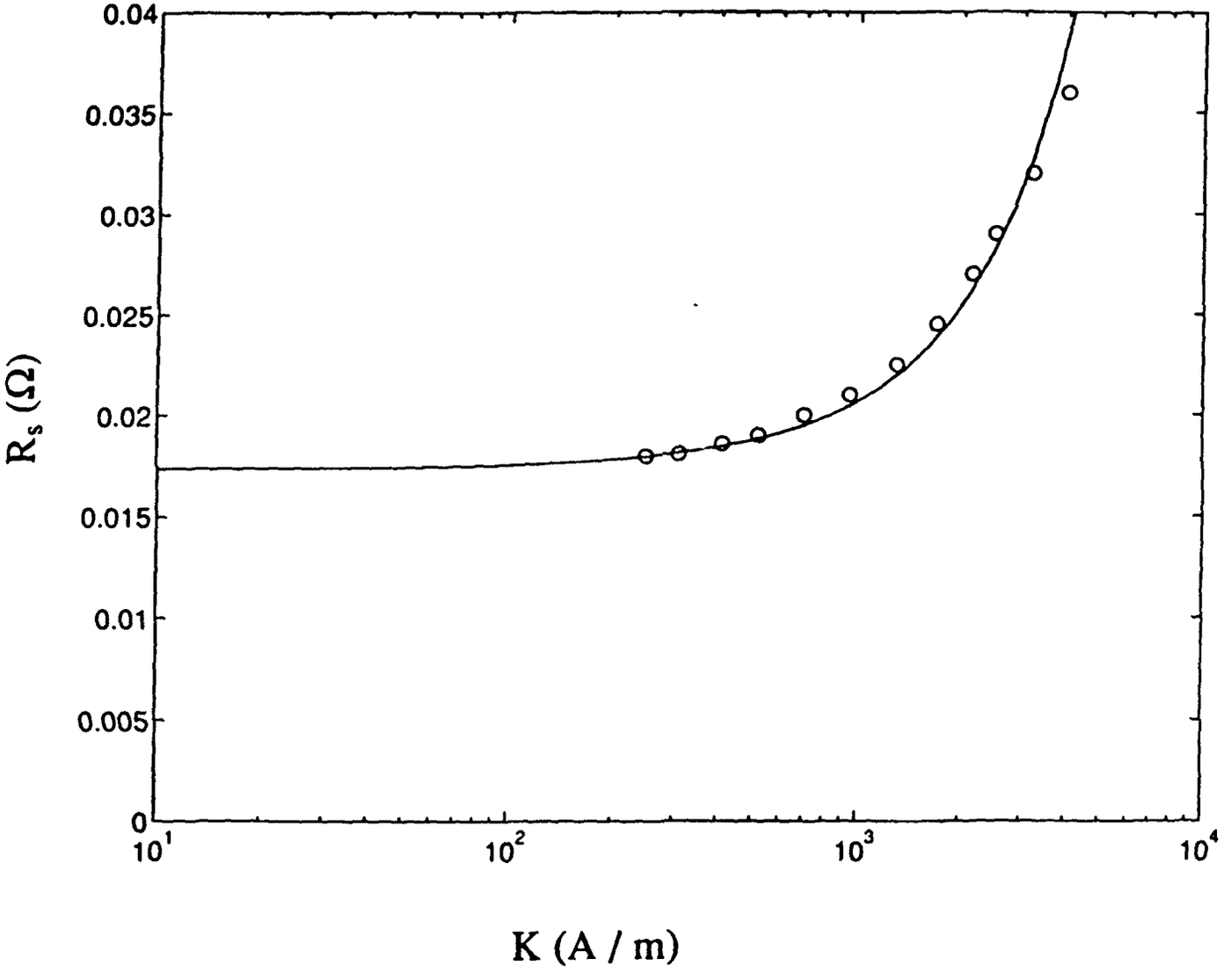

Fig 11

Office of Naval Research

DISTRIBUTION LIST

Arthur K. Jordan
Scientific Officer — 3 copies

Code: 1114SE
Office of Naval Research
800 North Quincy Street
Arlington, VA 22217

Administrative Contracting Officer — 1 copy
E19-628
Massachusetts Institute of Technology
Cambridge, MA 02139

Director — 1 copy
Naval Research Laboratory
Washington, DC 20375
Attn: Code 2627

Defense Technical Information Center — 2 copies
Bldg. 5, Cameron Station
Alexandria, VA 22314